Guidance of an Off-Road Tractor-Trailer System Using Model Predictive Control

by

James T. Salmon

A thesis submitted to the Graduate Faculty of
Auburn University
in partial fulfillment of the
requirements for the Degree of
Master of Science

Auburn, Alabama
December 14, 2013

Keywords: MPC, Coupled Ground Vehicles, Mobile Robots

Acknowledgments

I would like to dedicate this thesis to all my friends and family who supported me during my academic career, starting with my immediate family – my parents, Cyndy and Thad Salmon and my sister, Emily. Throughout the tough moments, you have always been there to keep me on the right track, you never gave up on me, and I don't think I would have made it anywhere near this point without you.

I also want to thank my extended family in Alabama. First, my grandparents, Cecil and Nell Prescott, as well as my grandmother, Mabel Salmon. Thank you for helping me in my move to Auburn. Thank you to my grandfather, Joseph T. Salmon Sr., who is no longer with us. You did some amazing things for our family, and you are greatly missed. Also, thank you to my aunts, uncles, and cousins out here who helped introduce me to Southern life. Watching football games with you have been great fun!

Next, I want to thank my advisor, Dr. David Bevly, for offering me a research assistantship position in the GAVLAB. Also, thank you to Dr. John Hung and Dr. Song-Yul Choe whom I consider co-advisors, for their guidance. Graduate school was challenging, but I learned a lot more about control systems than I ever knew existed, and I am confident that I would be able to contribute much as a controls engineer in my career to come.

Also, thank you to my colleagues in the GAVLAB, to all of my friends in Auburn, and to all of my friends in California. You all have been a positive influence on me throughout the years, and I wish you all the best.

Finally, I want to thank my great-great grandfather, Dr. Frederic C. Biggin, for his dedication to Auburn University. Your contributions in the Auburn School of Architecture set the stage for Auburn's development into the great institution it has become. Auburn is in good hands, it has a bright future ahead, and I am glad to be a part of it. War Eagle!

Table of Contents

List of Figures

List of Tables

List of Symbols

Δ	Angle Difference between Tractor and Trailer ($\Psi_1 - \Psi_2$)
δ	Front Tire Steering Angle of Tractor
$\dot{x}_1$	Forward Velocity of Tractor
$\dot{x}_2$, $\ddot{x}_2$	Forward Velocity and Acceleration of Trailer
$\dot{y}_1$, $\ddot{y}_1$	Lateral Velocity and Acceleration of Tractor
$\dot{y}_2$, $\ddot{y}_2$	Lateral Velocity and Acceleration of Trailer
Ψ_1, r_1, $\dot{r}_1$	Heading, Angular Velocity, and Angular Acceleration of Tractor
Ψ_2, r_2, $\dot{r}_2$	Heading, Angular Velocity, and Angular Acceleration of Trailer
θ_{path_j}	Angle between Trailer's current heading and closest path point (when finding cost)
θ_{pred_j}	Angle between Trailer's current heading and j-th Prediction Point (when finding cost)
a	Length from Tractor GPS (kinematic model) or CG (dynamic model) to front tire
b	Length from Tractor GPS (kinematic model) or CG (dynamic model) to back tire
c	Length from Tractor GPS (kinematic model) or CG (dynamic model) to hitch
C_1	Cornering Coefficient of the Front Tractor Tire
C_2	Cornering Coefficient of the Back Tractor Tire
C_3	Cornering Coefficient of the Trailer Tire
d	Length from Trailer GPS (kinematic model) or CG (dynamic model) to hitch

e	Length from Trailer GPS (kinematic model) or CG (dynamic model) to trailer tire
H'_x, H'_y	Forward and Lateral Hitch Forces (trailer side)
H_x, H_y	Forward and Lateral Hitch Forces (tractor side)
I_1	Yaw Inertia of the Tractor
I_2	Yaw Inertia of the Trailer
J'_i	Derivative of the i-th Cost
J_i	Cost of the i-th prediction
l_j	Shortest Length between j-th Prediction Point and Path (when finding cost)
m_1	Mass of the Tractor
m_2	Mass of the Trailer
w_j	Weight assigned to the j-th Prediction Point (when finding cost)
X_1, Y_1	Absolute X and Y Positions of Tractor
X_2, Y_2	Absolute X and Y Positions of Trailer
$X_{1,ref}$, $Y_{1,ref}$	Absolute X and Y Positions of Tractor (kinematic model)
$X_{2,ref}$, $Y_{2,ref}$	Absolute X and Y Positions of Trailer (kinematic model)
X_{path_j} Y_{path_j}	Closest Point on the Path to j-th Prediction Point (when finding cost)
$X_{trailer_j}$ $Y_{trailer_j}$	j-th Predicted X and Y Positions of Trailer (when finding cost)

Abstract

This thesis presents an effort to improve the path following reliability of a tractor-trailer system by using a non-linear Model Predictive Control (MPC) approach. The proposed method allows an autonomous mobile robot to make informed control decisions based on anticipating changes in the path conditions, rather than reacting to them, which could potentially reduce path following error on turns.

Using a non-linear tractor-trailer model, the controller takes the tractor's measured position and heading, as well as information about the path geometry in front of it, and it determines the optimal steer angle. Then, in the case of an Ackerman-steered vehicle, a secondary algorithm takes the desired steer angle and calculates the amount of voltage to apply to the steering wheel motor to achieve the steer angle. In comparison, a differential-steered, or skid-steered vehicle takes the set point (given as a turn rate in radians per second) and computes the voltages to the traction motors internally.

In the MATLAB simulation study, the controller algorithm is capable of guiding a 2-1/2 meter long trailer around a 5-meter radius turn, when towed by a four wheel drive off-road utility vehicle, with a maximum error of 8.5 centimeters. These results are highly idealized, however. Adding sensor noise and process noise in simulation increases the error, and inherent sensor bias and latency during the live run increases the error substantially.

From the experimental results, it is concluded that non-linear MPC has the potential to improve the reliability of the path following of a robot and trailer system. In order to fully reap the benefits of non-linear MPC however, the model has to be accurate, and the computer has to be fast enough to compute predictions from the model in real-time.

Chapter 1
Introduction

Model Predictive Control (MPC) is a relatively new control method, first practiced by Shell Oil, which determines an optimal input, called a set point, and then guides the system to that set point. It is a control technique that is commonly used in the oil industry, as well as other applications in chemical engineering. With advancements in computing power, engineers have begun exploring the usage of MPC to other applications, including autonomous vehicle control. However, due to the computational expense of MPC, especially when a nonlinear model is used, most vehicular applications are limited to low-speed operation [1].

For many off-road vehicle applications however, low-speed operation is the norm. In agriculture, tractor-trailer systems are used to spread seed, fertilizer and top soil. In the case of the Department of Defense, a tractor pulls a fiberglass trailer that carries metal sensors to scan the ground for unexploded ordnance, which is further explained in [2]. Despite the computational expense of MPC, these applications involve process that are slow enough for MPC to produce good results.

1.1 Background

Auburn University, with the support of the U.S. Army Corps of Engineers, has been researching ways to control off-road tractor-trailer systems for conducting geophysical surveys, with the trailer being the object of interest for control. A geophysical survey involves a scan of a given area in search of metal objects in the ground [9].

In an effort to streamline the U.S. Military, the Department of Defense (DOD) has initiated numerous military base closures around the United States. Many of these bases contained training sites for tactical strategies that are less commonly used in modern military operations. According to [3], the DOD closed or realigned over 800 defense locations and relocated over 125,000 personnel since 2005, in an operation called Base Realignment and Closure (BRAC). When a base closes, the land is sold to private developers. However, there are legitimate safety concerns regarding unexploded ordnance (UXO) still remaining on plots of land that used to be training sites.

To ensure that a questionable field is safe, the Army Corps of Engineers conducts geophysical surveys to look for potential UXO. While there have been no recorded incidents of injuries or fatalities during these surveys due to accidental discharge, the risk is still a concern. This is why the Army Corps of Engineers has tasked Auburn University in developing an unmanned robot vehicle that would carry out the task of searching for UXO. Auburn has since used a setup consisting of a GPS guided trailer made of fiberglass, towed by a tractor [5], which would allow the scanning of the ground for metal objects without interference from the metal inside the tractor.

1.2 Previous Work at Auburn University

Previously, linear state feedback controllers [9], LQG controllers [10], and hybrid backstepping controllers [11] were used in the guidance of the surveying system. In all cases, these control methods work very well in guiding the trailer to the path, as long as the path is straight. However, due to the complexity of tractor-trailer system dynamics, keeping the trailer on the path becomes much more difficult when going around turns. The most accurate controller found so far was the linear state feedback controller, which had a maximum recovery error of 20.4cm [9]. Conversely, the hybrid backstepping controller had maximum errors of up to 40cm [11], and the LQG controller had maximum errors of around 44cm [10]. Both authors conclude, however, that these errors might be improved by fine-tuning the gains.

This thesis proposes, on the other hand, that the biggest source of error is the nonlinearity of a tractor-trailer hitch connection. According to [14], when the angle between

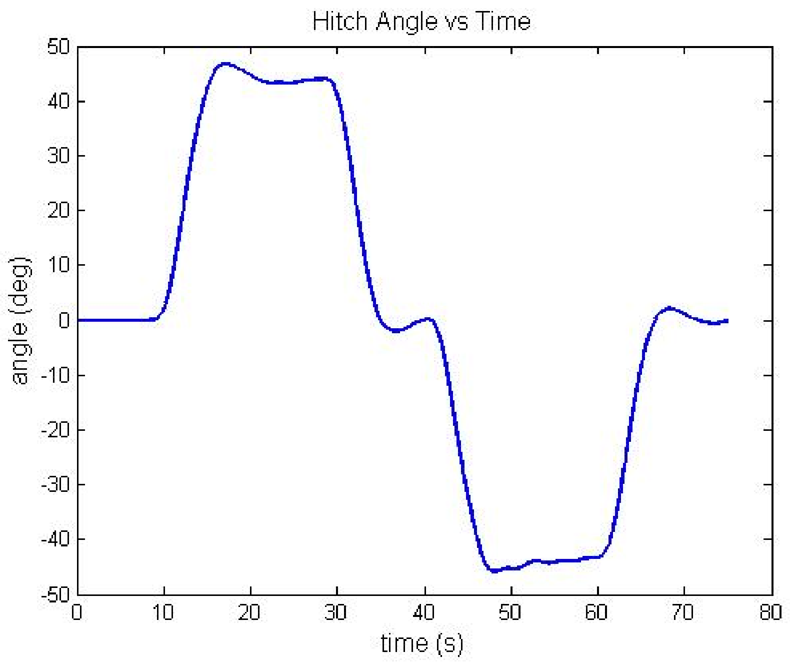

Figure 1.1: Hitch Angle vs Time

the tractor and the trailer exceeds 7°, linearized tractor-trailer models become less accurate. Figure 1.1 shows a time plot of the hitch angle, where the maximum hitch angle reaches 47.8° as a simulated tractor-trailer system navigates an S-curve with turn radii of 5 meters.

The biggest issue during a geophysical survey is recovering out of a turn. As seen in Figure 1.2, the robot overshoots the beginning of the straight sections of the desired path, and then it corrects itself. In the case of Figure 1.3, the robot overcompensates and undergoes an oscillatory correction maneuver to return to the desired path. Finally, in Figure 1.4, the robot does a combination of overshooting the straight section reentries, as well as overcompensating for errors. With these errors, the ground scanners on the trailer could potentially miss locations on the ground that contain critical information.

In each of the afore-mentioned works, the robot follows what is known as a "Dubins path." According to Lester E. Dubins, the shortest path between two oriented points consists of straight lines and turns of constant radii [4]. However, dynamic constraints make it infeasible for a non-holonomic trailer to follow a path perfectly where the curvature changes instantaneously. One way to address this problem is to design paths with clothoid turns,

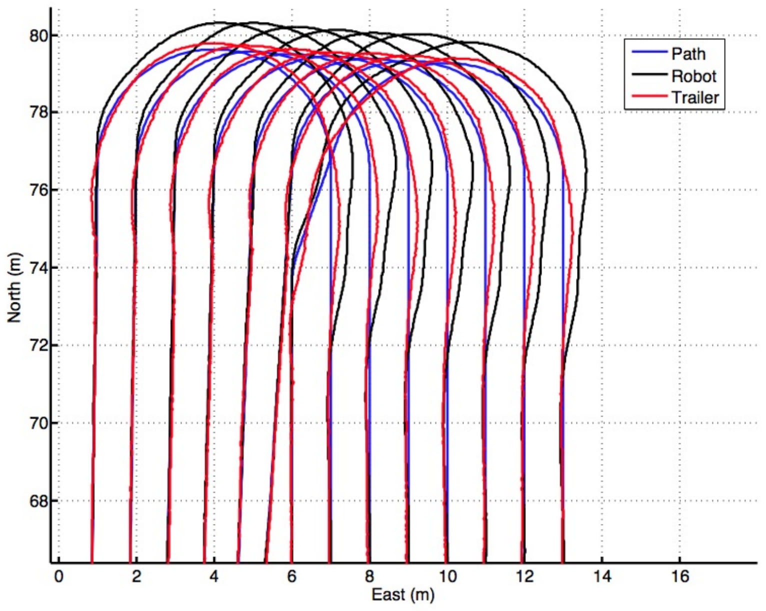

Figure 1.2: Path Following Using Linear State Feedback [9]

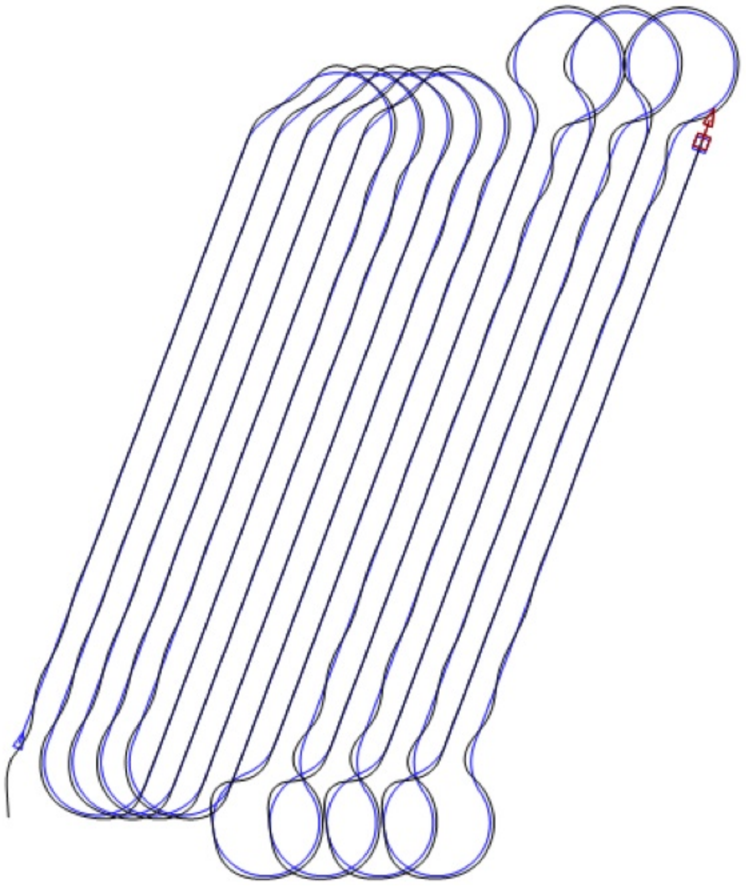

Figure 1.3: Path Following Using LQG [10]

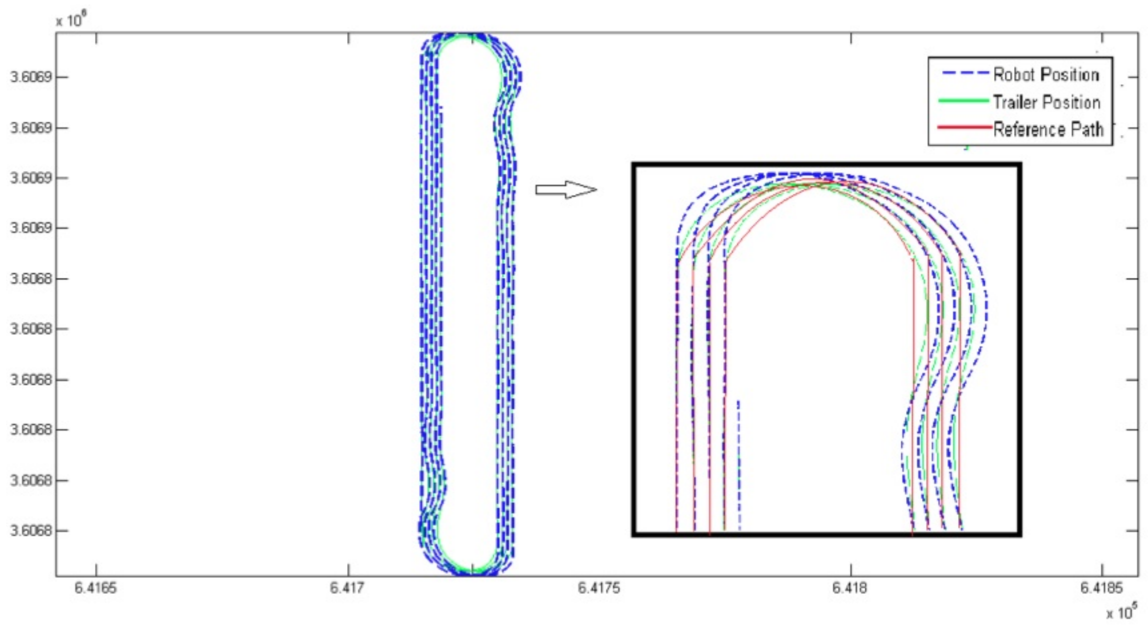

Figure 1.4: Path Following Using Hybrid Backstepping [11]

as studied in [6]. A clothoid is an arc where the curvature changes linearly, as opposed to instantaneously. They are commonly used in highway and railway design, and several clothoid computation algorithms exist, such as the one introduced in [7]. For each of the experiments done in this thesis, however, a constant radius turn will be used. This will force an error into the system intentionally, and it would allow the controller's recovery performance to be measured.

1.3 Proposing Model Predictive Control as a Potential Solution

The goal of this research is to develop a control algorithm that will improve the guidance of a trailer to a desired path during and after making a turn. Unlike the controllers previously used at Auburn University which choose guidance inputs based on the trailer's *current* position relative to the path, this thesis proposes designing a model predictive controller that chooses guidance inputs based on where the trailer is predicted to go, based upon a model. This is similar to the way a human drives a car, as a human subconsciously predicts where

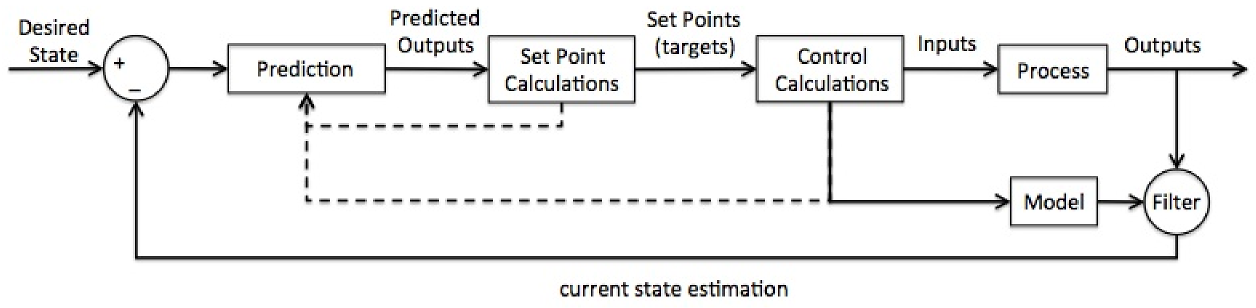

Figure 1.5: A Model Predictive Control Flowchart [8]

his or her car is going to go given a forward and steering input, and then the human adjusts the forward and steering controls of the car accordingly.

Of course, it is fair to ask the question of whether or not a computer can make model calculations fast enough to determine the optimal control inputs. After all, if a computer takes too long to predict an optimal solution, the control system becomes useless. Also, if the model is oversimplified, a model predictive controller's performance would be no better than a classical controller. For this application, however, the robot moves at a forward speed of 1 meter per second. Because of the low speed of the system, inertial properties as well as tire slip properties of the tractor and trailer will be ignored, and a simplified kinematic tractor-trailer model will be used, making the nonlinear MPC calculations feasible.

In general, MPC follows an algorithm depicted by the flowchart in Figure 1.5. First, the controller makes a prediction, choosing a particular steer angle. Then, using a model of the system, the controller looks at where the trailer will go if the robot uses that steer angle. It will then compare the result to the desired path. If the result does not meet tolerance specifications, it will make another prediction. Otherwise, the controller will use this steer angle (now called a set-point) as a target angle to move the steering wheel to. The controller then determines the voltage into the steering motor by making control calculations, and it feeds that voltage into the motor. The controller also runs the input back through the model and compares the result from the process's feedback sensors (in this case, a GPS receiver).

1.4 Outline

This thesis introduces a numerical approach to a non-linear feedforward control problem, and it stresses real-time feasibility. It is necessary for the control system to determine inputs quickly, while maintaining a high degree of accuracy. Two tractor-trailer models are presented in Chapter 2. The first, a 4th-order kinematic model, is a standard control model that is currently being used at Auburn University. The second model, a 9th-order bicycle model, has not been used at Auburn yet, due to its complexity and difficulty for a computer to numerically compute in real-time. Chapter 3 presents the numerical MPC method responsible for choosing the appropriate set points, and it shows how these set points can be achieved through classical control method design. Chapter 4 includes results from computer simulations with the two competing tractor-trailer models described in Chapter 2, as well as results from an experimental run on a Segway RMP 400. Finally, Chapter 5 presents conclusions from the results of this work and proposes future work.

Chapter 2

Kinematic and Dynamic Modeling of the System

This chapter presents the derivation of the aforementioned tractor-trailer models. First, a kinematic model is derived for a front-steering tractor, as well as a skid-steering tractor, towing a trailer. Then, a dynamic bicycle model for the same system is derived using Newtonian mechanics. The chapter then closes with a discussion on why the kinematic model is preferable for MPC with present technology, but also how the dynamic model would be preferable in other scenarios.

2.1 Kinematic Model

The kinematic model is a basic, "no-frills" model that can satisfy the prediction requirement for Model Predictive Control in low-speed applications. The primary advantage to using a kinematic model is its simplicity. A computer could numerically integrate a kinematic model accurately, using a much larger time step than when numerically integrating a dynamic model. The disadvantage of a kinematic model is that it assumes (1) the ground is perfectly flat, (2) the tires have perfect traction with the ground (no slip), and (3) it ignores inertia and lateral forces. Due to the low-speed operation during a geophysical survey, making these assumptions do not impact the accuracy of the predictions significantly.

2.1.1 List of Parameters & Velocity Diagram

Table 2.1 describes the variables used for a Kubota RTV, while Figure 2.1 shows the connected tractor-trailer system.

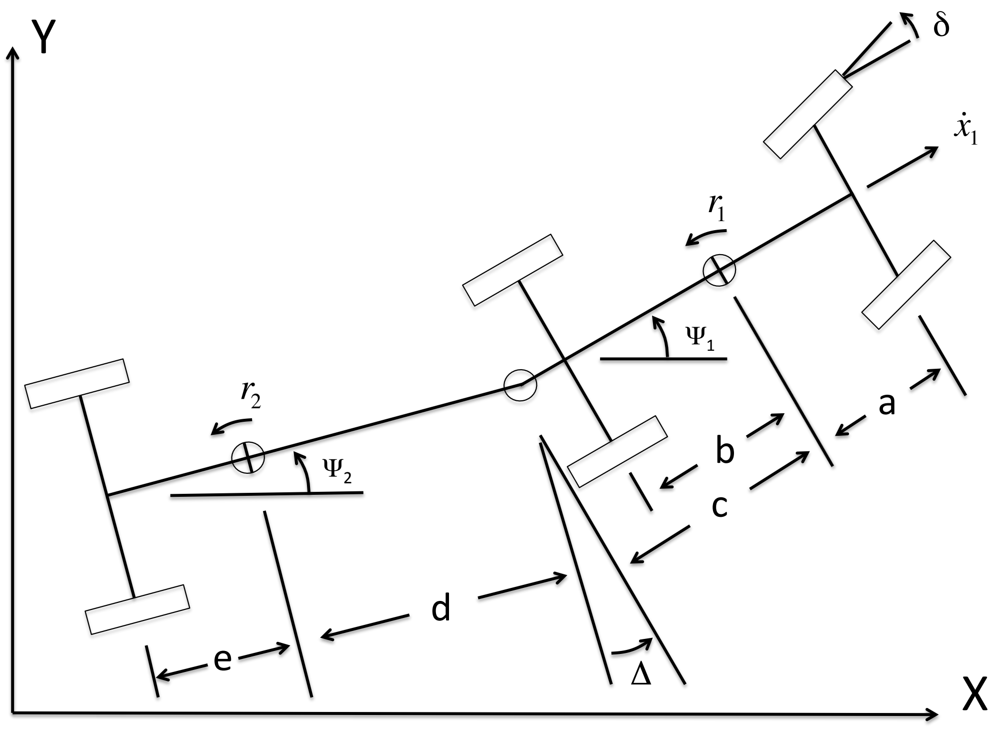

Figure 2.1: Schematic for a Tractor-Trailer System Kinematic Model

Parameter	Description	Value (if constant)
$X_{1,ref}$	Absolute X Position of Tractor	variable
$Y_{1,ref}$	Absolute Y Position of Tractor	variable
$X_{2,ref}$	Absolute X Position of Trailer	variable
$Y_{2,ref}$	Absolute Y Position of Trailer	variable
X_1	Absolute X Position of Tractor (back axle)	variable
Y_1	Absolute Y Position of Tractor (back axle)	variable
$\dot{x}_1$	Forward Velocity of the Tractor	1 m/s
Ψ_1, r_1	Heading and Angular Velocity of Tractor	variable
Ψ_2, r_2	Heading and Angular Velocity of Trailer	variable
δ	Front Tire Steering Angle of Tractor	variable
Δ	Angle Difference between Tractor and Trailer ($\Psi_1 - \Psi_2$)	$\Psi_1 - \Psi_2$
a	Length from Tractor GPS receiver to center of front tire	0.75 m
b	Length from Tractor GPS receiver to center of back tire	1.21 m
c	Length from Tractor GPS receiver to hitch	1.74 m
d	Length from Trailer GPS receiver to hitch	3.0 m
e	Length from Trailer GPS receiver to trailer tire	1.0 m

Table 2.1: List of Tractor-Trailer System Parameters (kinematic model)

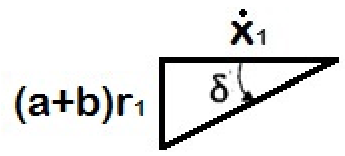

Figure 2.2: Steering to Angular Velocity

2.1.2 Kinematic Model Derivation

Considering the tractor coordinates first, it is assumed that there is no lateral velocity at the back axle of the tractor. Using this assumption, the tractor's angular velocity can then be related to its forward velocity and the steering angle of the front tire as shown in Figure 2.2, which leads to Equation (2.1).

$$r_1 = \frac{\dot{x}_1 \tan \delta}{(a+b)} \tag{2.1}$$

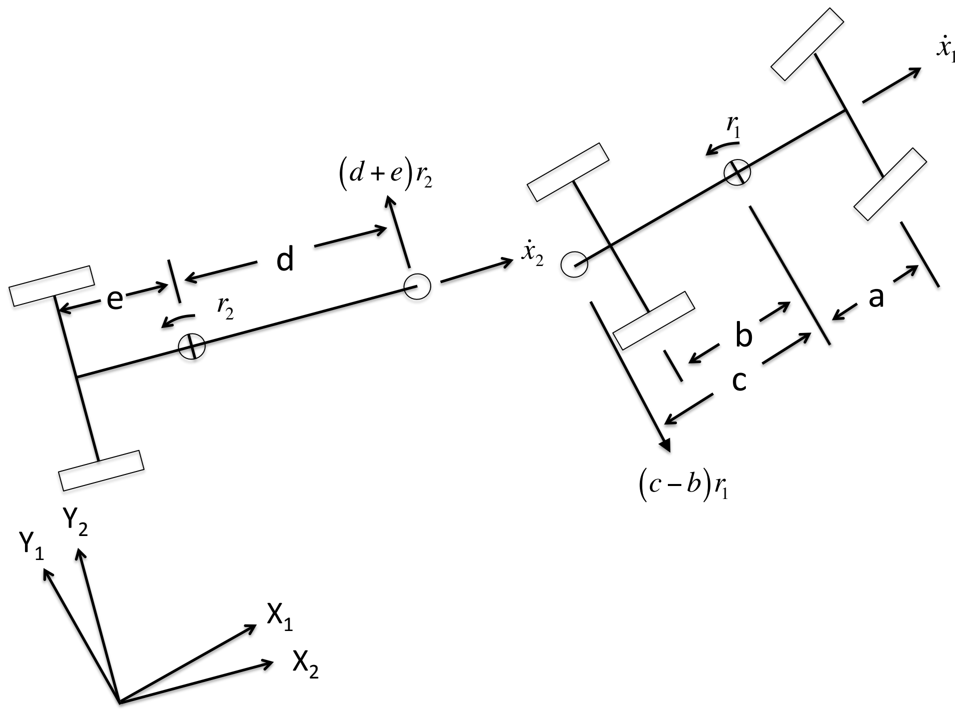

Figure 2.3: Tractor and Trailer Hitch Velocities

Next, by studying Figure 2.3, the forward and lateral velocities at the hitch are found relative to both the tractor and the trailer.

Velocity of the hitch in tractor coordinates: $\dot{x}_1\hat{i}_1 - (c-b)r_1\hat{j}_1$

Velocity of the hitch in trailer coordinates: $\dot{x}_2\hat{i}_2 + (d+e)r_2\hat{j}_2$

These two velocity expressions both describe the same velocity, and therefore, they can be related to each other using a rotation matrix:

$$\begin{bmatrix} \dot{x}_2 \\ (d+e)r_2 \end{bmatrix} = \begin{bmatrix} \cos\Delta & \sin\Delta \\ \sin\Delta & -\cos\Delta \end{bmatrix} \begin{bmatrix} \dot{x}_1 \\ (c-b)r_1 \end{bmatrix} \tag{2.2}$$

An equation for the angular velocity of the trailer can be extracted from the above relation as shown in Equation (2.3):

$$r_2 = \frac{\dot{x}_1}{(d+e)}\sin\Delta - \frac{(c-b)r_1}{(d+e)}\cos\Delta \tag{2.3}$$

While an equation for the forward velocity of the tractor could be extracted from the matrix rotation, it is unnecessary to do so. Instead, by finding the tractor's global position and considering the headings of both the tractor and the trailer, the trailer's global position can be found as well. This eliminates several integration steps, and it allows for a larger numerical integration time step size. Equations (2.4) and (2.5) show the translation to global coordinates for the tractor.

$$\dot{X}_1 = \dot{x}_1 \cos\Psi_1 \tag{2.4}$$

$$\dot{Y}_1 = \dot{y}_1 \sin\Psi_1 \tag{2.5}$$

To summarize the derivation so far, Equations (2.1), (2.4), and (2.5) give the position and heading of the back axle of the tractor, while Equation (2.3) gives the angular velocity of the trailer. Now, some kinematic relations are considered to locate the points of interest (i.e. the GPS receivers) on both the tractor and the trailer. Equations (2.6) and (2.7) give the antenna location on the tractor:

$$X_{1,ref} = X_1 + b \cos \Psi_1 \tag{2.6}$$

$$Y_{1,ref} = Y_1 + b \sin \Psi_1 \tag{2.7}$$

Finally, the trailer's GPS receiver location can be calculated using the following Equations (2.8) and (2.9):

$$X_{2,ref} = X_{1,ref} - c \cos \Psi_1 - d \cos \Psi_2 \tag{2.8}$$

$$Y_{2,ref} = Y_{1,ref} - c \sin \Psi_1 - d \sin \Psi_2 \tag{2.9}$$

2.1.3 Skid-Steer Vehicle Modification

Many skid-steer vehicles, such as the Segway Robotics Mobility Platform (RMP) 400, have an existing steering control system that only requires an angular velocity input, removing the need for Equation (2.1). However, there is often a time delay between the angular velocity input, and when the robot reaches that angular velocity. The design of a compensator for this delay will be addressed in Chapter 3.

2.2 Dynamic Bicycle Model

The dynamic bicycle model introduces the possibility of adding exterior input forces to the model, such as bumps and dips in the ground. The major difference in the model

Parameter	Description	Value
X_1	Absolute X Position of Tractor (center of gravity)	variable
Y_1	Absolute Y Position of Tractor (center of gravity)	variable
X_2	Absolute X Position of Trailer (center of gravity)	variable
Y_2	Absolute Y Position of Trailer (center of gravity)	variable
$\dot{x}_1$	Forward Velocity of Tractor	1 m/s
$\dot{y}_1$,$\ddot{y}_1$	Lateral Velocity and Acceleration of Tractor	variable
$\dot{x}_2, \ddot{x}_2$	Forward Velocity and Acceleration of Trailer	variable
$\dot{y}_2, \ddot{y}_2$	Lateral Velocity and Acceleration of the Trailer	variable
$\Psi_1, r_1, \dot{r}_1$	Heading, Angular Velocity, and Angular Acceleration of Tractor	variable
$\Psi_2, r_2, \dot{r}_2$	Heading, Angular Velocity, and Angular Acceleration of Trailer	variable
H_x, H_y	Forward and Lateral Hitch Forces (tractor side)	variable
H'_x, H'_y	Forward and Lateral Hitch Forces (trailer side)	variable
δ	Front Tire Steering Angle of Tractor	variable
Δ	Angle Difference between Tractor and Trailer ($\Psi_1 - \Psi_2$)	$\Psi_1 - \Psi_2$
a	Length from Tractor CG to center of front tire	0.75 m
b	Length from Tractor CG to center of back tire	1.21 m
c	Length from Tractor CG to hitch	1.74 m
d	Length from Trailer CG to hitch	3.0 m
e	Length from Trailer CG to trailer tire	1.0 m
m_1	Mass of the Tractor	1225 kg
I_1	Yaw Inertia of the Tractor	$m_1 \cdot a \cdot b$
m_2	Mass of the Trailer	30 kg
I_2	Yaw Inertia of the Trailer	$m_2 \cdot d \cdot e$
C_1	Cornering Coefficient of the Front Tractor Tire	$80 \cdot m_1$
C_2	Cornering Coefficient of the Back Tractor Tire	$80 \cdot m_1$
C_3	Cornering Coefficient of the Trailer Tire	$80 \cdot m_2$

Table 2.2: List of Tractor-Trailer System Parameters (dynamic model)

assumptions is that the tires no longer have perfect traction with the ground, and they have to push against the ground in order to control a vehicle's direction. These advantages come at a cost, however, as the numerical computation requires a significantly smaller time step size than the kinematic model.

2.2.1 List of Parameters and Acceleration/Force Diagram

Table 2.2 describes the variables used for a Kubota RTV, while Figure 2.4 shows the connected tractor-trailer system.

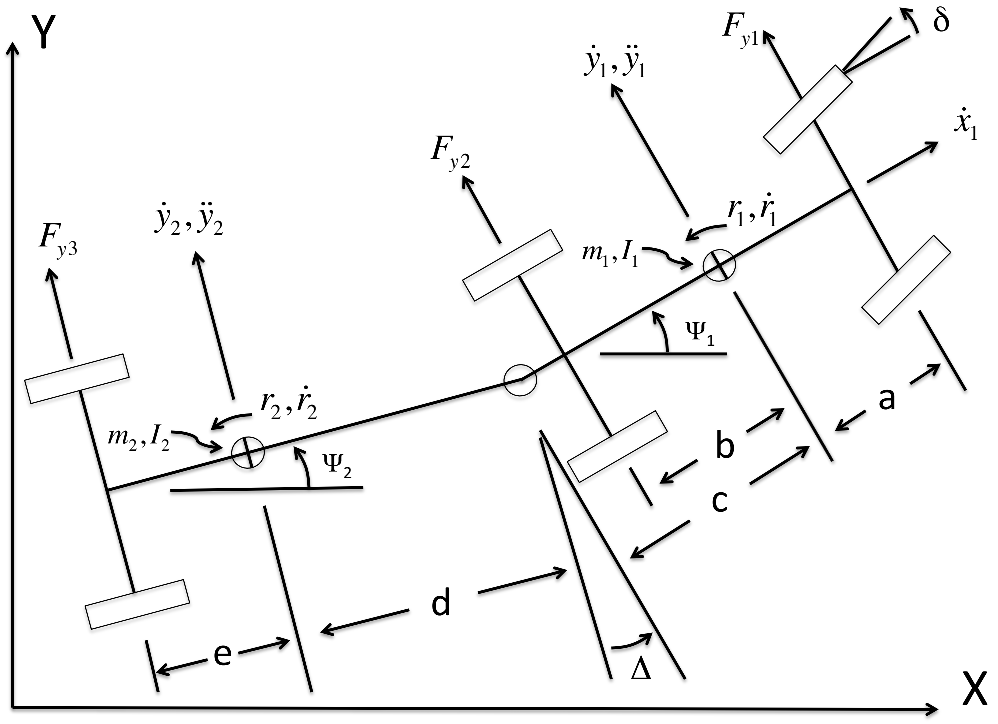

Figure 2.4: Schematic for a Tractor-Trailer System Dynamic Model

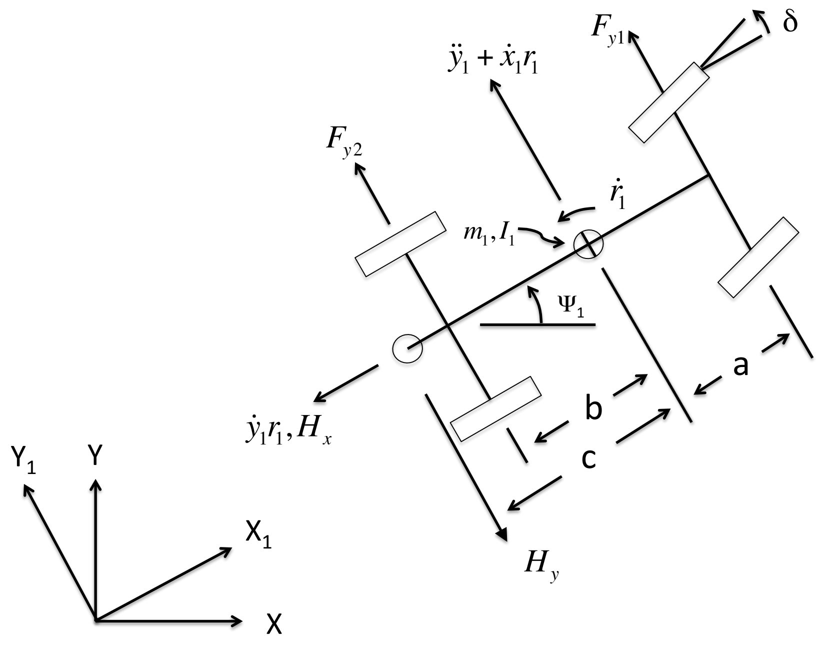

Figure 2.5: Tractor Accelerations and Forces

2.2.2 Force and Acceleration Analysis on Tractor and Trailer

As seen in Figure 2.5, the tractor has three lateral forces acting on it: two produced by the tires, and a lateral force produced at the hitch. There are two lateral acceleration components influenced by these forces – a lateral perturbed acceleration $\ddot{y}_1$, and a centripetal acceleration $\dot{x}_1 r_1$. These forces and accelerations relate as described by Equations (2.10) and (2.11), using Newtonian mechanics.

$$m_1\ddot{y}_1 + m_1\dot{x}_1 r_1 = F_{y1} + F_{y2} - H_y \tag{2.10}$$

$$I_1\dot{r}_1 = aF_{y1} - bF_{y2} + cH_y \tag{2.11}$$

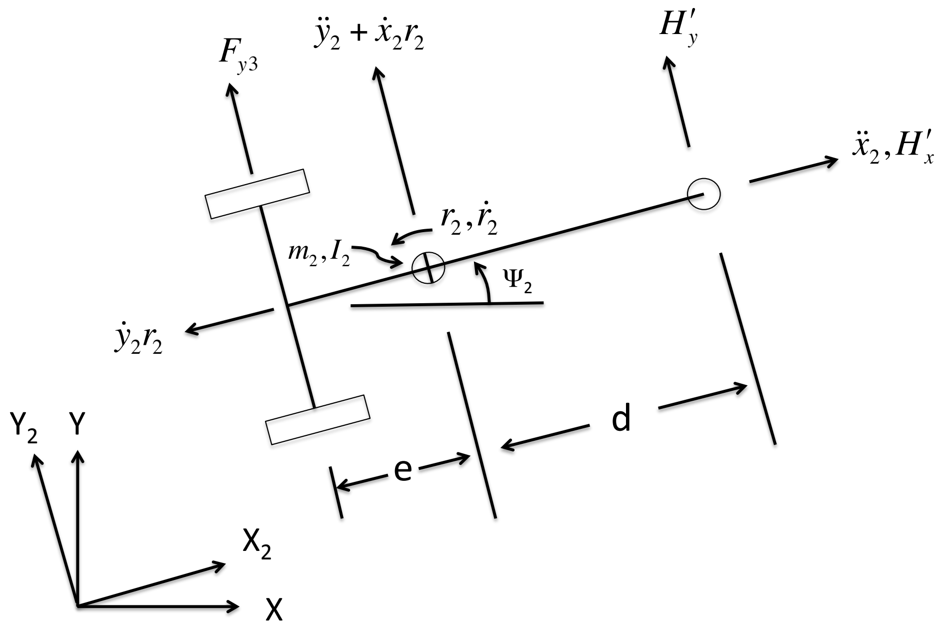

Figure 2.6: Trailer Accelerations and Forces

Next, the trailer's accelerations and forces are examined as seen in Figure 2.6. In similar fashion to the tractor equations, Equations (2.12) and (2.13) describe the lateral motion of the trailer.

$$m_2\ddot{y}_2 + m_2\dot{x}_2 r_2 = F_{y3} + H'_y \tag{2.12}$$

$$I_2\dot{r}_2 = dH'_y - eF_{y3} \tag{2.13}$$

Unlike the tractor, which was said to have a constant forward velocity (and hence no forward acceleration), the trailer does have a forward acceleration component. Equation (2.14) describes this motion:

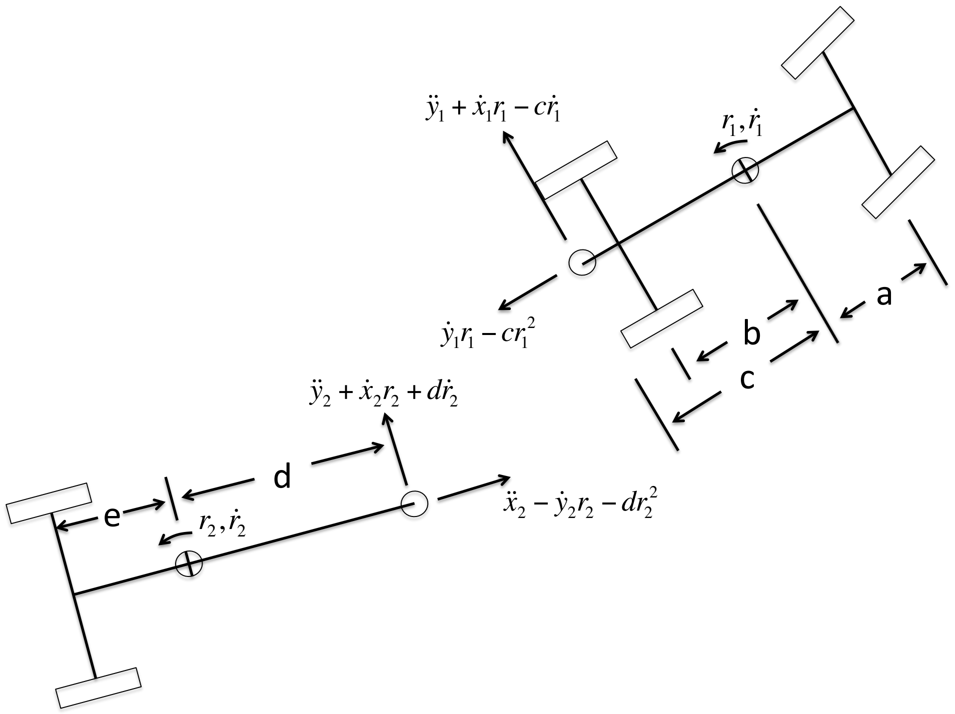

$\ddot{y}_1 + \dot{x}_1 r_1 - c\dot{r}_1$
$r_1, \dot{r}_1$
$\dot{y}_1 r_1 - c r_1^2$
a
b
c
$\ddot{y}_2 + \dot{x}_2 r_2 + d\dot{r}_2$
d
e
$r_2, \dot{r}_2$
$\ddot{x}_2 - \dot{y}_2 r_2 - d r_2^2$

Figure 2.7: Tractor & Trailer Hitch Accelerations

$$m_2\ddot{x}_2 - m_2\dot{y}_2 r_2 = H'_x \tag{2.14}$$

2.2.3 Relative Forces and Accelerations

To relate the dynamic tractor and trailer models, similarly to the kinematic model, the accelerations at the hitch can be determined with respect to both the tractor and the trailer separately (see Figure 2.7), so they can be related using a rotation matrix (Equation (2.15)).

$$\begin{bmatrix} \ddot{x}_2 - (\dot{y}_2 r_2 + d r_2^2) \\ \ddot{y}_2 + \dot{x}_2 r_2 + d\dot{r}_2 \end{bmatrix} = \begin{bmatrix} \cos\Delta & -\sin\Delta \\ \sin\Delta & \cos\Delta \end{bmatrix} \begin{bmatrix} -(\dot{y}_1 r_1 - c r_1^2) \\ \ddot{y}_1 + \dot{x}_1 r_1 - c\dot{r}_1 \end{bmatrix} \tag{2.15}$$

Using the same rotation matrix as Equation (2.15), Equation (2.16) relates the forces. Note that by Newton's Third Law, the force acting on the hitch from the perspective of the

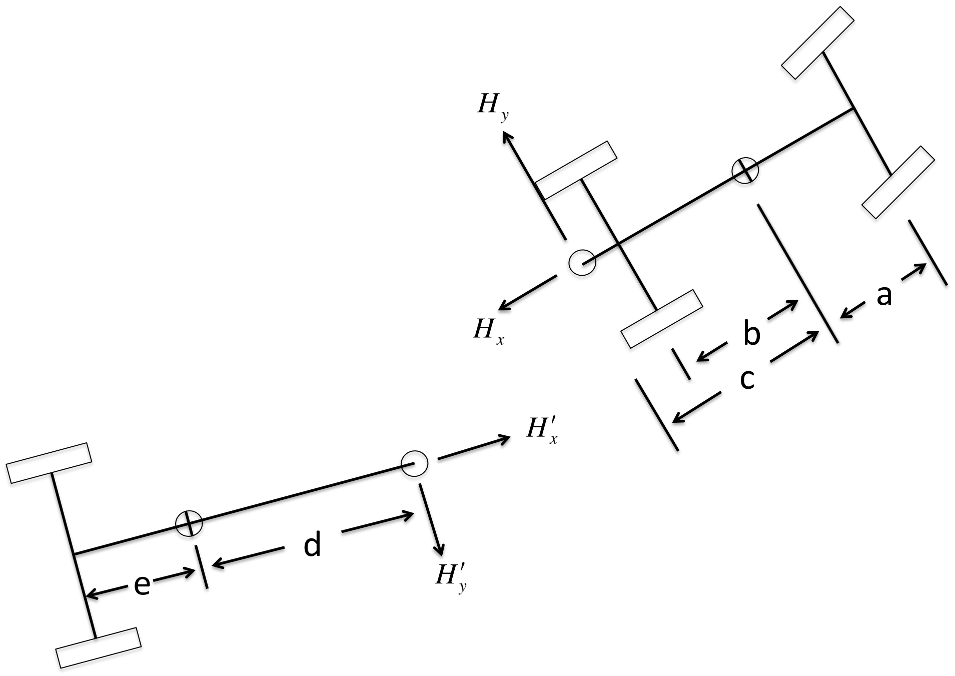

Figure 2.8: Hitch Forces

tractor has to be *equal and opposite* to the force acting on the hitch from the perspective of the trailer, as shown in Figure 2.8.

$$\begin{bmatrix} H'_x \\ H'_y \end{bmatrix} = \begin{bmatrix} \cos\Delta & -\sin\Delta \\ \sin\Delta & \cos\Delta \end{bmatrix} \begin{bmatrix} H_x \\ H_y \end{bmatrix} \tag{2.16}$$

2.2.4 Tire Model Derivation

Historically, tires have been difficult for engineers to model accurately. In most cases, tire models are derived experimentally, as opposed to theoretically. For this model, however, a somewhat non-intuitive approach called the “slip angle” model is used. The slip angle concept does not imply skidding, but instead implies that as tires roll and experience a lateral force, some portions of the tire begin to slip from their point of contact with the

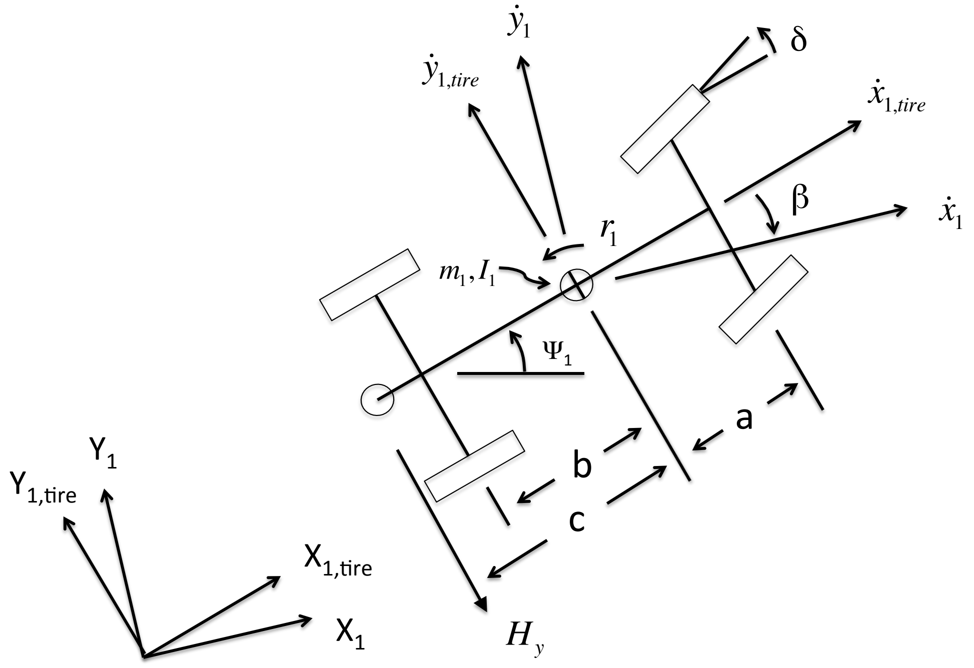

Figure 2.9: Tractor Motion from Tire Coordinate Frame

ground, while other portions of the tire are still essentially "locked" to the ground by static friction. For a more comprehensive description of the slip angle concept, refer to [12].

When a vehicle is traveling straight, there is virtually no difference between a vehicle's velocity and a tire's velocity. However, if a perturbation is introduced in the vehicle's movement, the tire will react based on its motion relative to the vehicle.

Figure 2.9 shows an exaggeration of a vehicle's perturbed motion from the coordinate frame of the tire. For the following calculations, $\dot{x}$ will be the tire's in-line rolling velocity, $\dot{y}$ will be the tire's lateral velocity, and Ψ will be the angle difference between the vehicle's forward motion and its lateral motion.

From Figure 2.9, the motion of the rear tractor tire can be related to the motion of the vehicle as shown in Equations (2.17), (2.18), and (2.19).

$$\beta_1 = \arctan\left(\frac{-\dot{y}_1}{\dot{x}_1}\right) \tag{2.17}$$

$$\dot{x} = \dot{x}_1 \cos\beta_1 + \dot{y}_1 \sin\beta_1 \tag{2.18}$$

$$\dot{y} = -\dot{x}_1 \sin\beta_1 + \dot{y}_1 \cos\beta_1 - br_1 \tag{2.19}$$

The force produced by the tire is the arctangent of the ratio between the lateral tire velocity $\dot{y}$ to its rolling velocity $\dot{x}$, multiplied by the negative of the cornering coefficient (Equation (2.20)).

$$F_{y2} = C_2 \arctan\left(\frac{-\dot{x}_1 \sin\beta_1 + \dot{y}_1 \cos\beta_1 - br_1}{\dot{x}_1 \cos\beta_1 + \dot{y}_1 \sin\beta_1}\right) \tag{2.20}$$

Similarly, without any steering angle, the front tire force would be modeled with Equation (2.21).

$$F_{y1} = C_1 \arctan\left(\frac{-\dot{x}_1 \sin\beta_1 + \dot{y}_1 \cos\beta_1 + ar_1}{\dot{x}_1 \cos\beta_1 + \dot{y}_1 \sin\beta_1}\right) \tag{2.21}$$

Conversely, if a steering angle is included, the front tire force would be modeled with Equation (2.22).

$$F_{y1} = C_1 \arctan\left(\frac{-\dot{x}_1 \sin(\beta_1 + \delta) + \dot{y}_1 \cos(\beta_1 + \delta) + ar_1 \cos\delta}{\dot{x}_1 \cos(\beta_1 + \delta) + \dot{y}_1 \sin(\beta_1 + \delta) + ar_1 \sin\delta}\right) \cos\delta \tag{2.22}$$

Finally, in similar fashion to Equation (2.20), the trailer tire force is modeled by Equation (2.23).

$$F_{y3} = C_3 \arctan\left(\frac{-\dot{x}_2 \sin\beta_2 + \dot{y}_2 \cos\beta_1 - er_2}{\dot{x}_2 \cos\beta_2 + \dot{y}_2 \sin\beta_2}\right) \tag{2.23}$$

2.2.5 Equations Collected & Translation to Global Coordinates

Now that the tractor trailer model equations of motion have been derived, Equations (2.10) through (2.16) can be combined to make Equations (2.24) through (2.28). The individual state variables can be isolated by applying Cramer's Method.

$$m_1\ddot{y}_1 + m_2\ddot{y}_2\cos\Delta - m_2\ddot{x}_2\sin\Delta = F_{y1} - m_1\dot{x}_1 r_1 + F_{y2} - (m_2\dot{x}_2 r_2 - F_{y3})\cos\Delta - m_2\dot{y}_2 r_2\sin\Delta \tag{2.24}$$

$$I_1\dot{r}_1 - cm_2\ddot{y}_2\cos\Delta + cm_2\ddot{x}_2\sin\Delta = aF_{y1} - bF_{y2} + c\left(m_2\dot{x}_2 r_2 - F_{y3}\right)\cos\Delta + cm_2\dot{y}_2 r_2\sin\Delta \tag{2.25}$$

$$dm_2\ddot{y}_2 - I_2\dot{r}_2 = (d+e)\,F_{y3} - dm_2\dot{x}_2 r_2 \tag{2.26}$$

$$\ddot{y}_1\sin\Delta - c\dot{r}_1\sin\Delta + \ddot{x}_2 = -\dot{x}_1 r_1\sin\Delta - \left(\dot{y}_1 r_1 - cr_1^2\right)\cos\Delta + \dot{y}_2 r_2 + dr_2^2 \tag{2.27}$$

$$\ddot{y}_1\cos\Delta - c\dot{r}_1\cos\Delta - \ddot{y}_2 - d\dot{r}_2 = -\dot{x}_1 r_1\cos\Delta + \left(\dot{y}_1 r_1 - cr_1^2\right)\sin\Delta + \dot{x}_2 r_2 \tag{2.28}$$

Finally, to translate each vehicle component from local to global coordinates, the following rotation is used:

$$\begin{bmatrix} \dot{X}_i \\ \dot{Y}_i \end{bmatrix} = \begin{bmatrix} \cos\theta_i & -\sin\theta_i \\ \sin\theta_i & \cos\theta_i \end{bmatrix} \begin{bmatrix} \dot{x}_i \\ \dot{y}_i \end{bmatrix} \tag{2.29}$$

where $i = 1$ for the tractor, and $i = 2$ for the trailer.

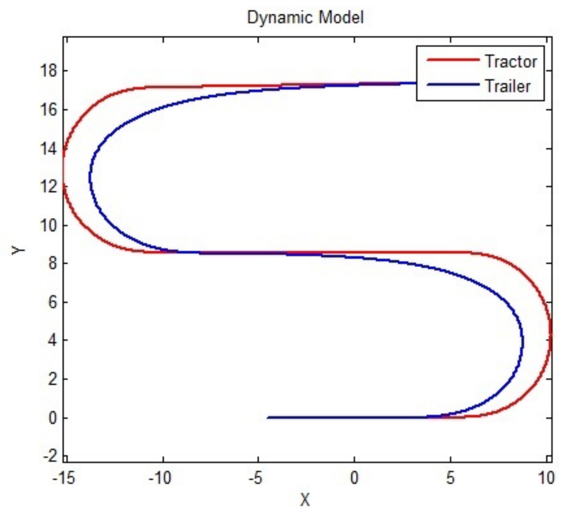

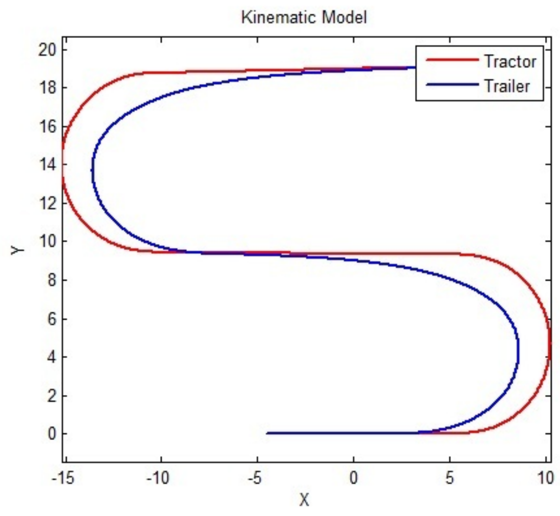

Figure 2.10: Dynamic Model vs Kinematic Model

2.3 Discussion

Both the kinematic and dynamic models were tested using MATLAB. Using a 4th-order Runge Kutta approximation, the kinematic model can produce an accurate estimate (<0.01% error) using a time step size of 0.025 seconds. On the other hand, the dynamic model requires a step size of 0.0001 seconds using a 6th-order Runge Kutta approximation to achieve an accurate estimate. Depending on the speed of the computer, the small step size required for the dynamic model could hinder the viability of using the model with MPC.

Fortunately, both models allow for a test of MPC when there is model error. Figure 2.10 shows these two models being run using a starting point where the CG of the tractor is at the origin, a forward velocity of 1m/s, and a common set of steering instructions that would guide the tractor around an S-curve. These models produce similar results, but they are by no means the same. Figure 2.11 shows how the models deviate as they go into the first turn, and after 6 seconds of a hard turn to the left, the models deviate by about 0.25 meters.

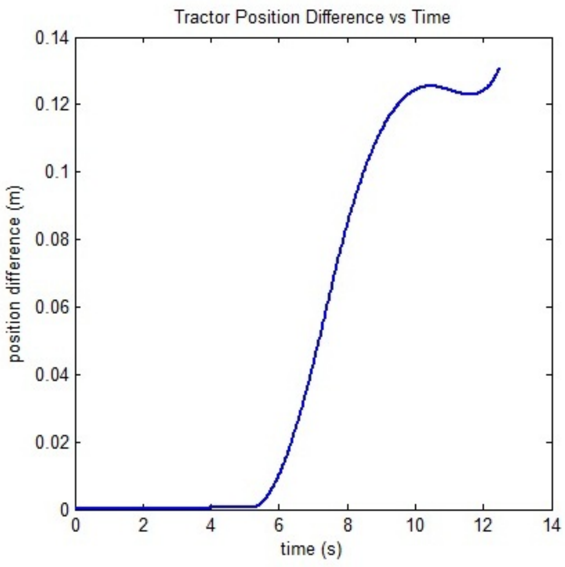

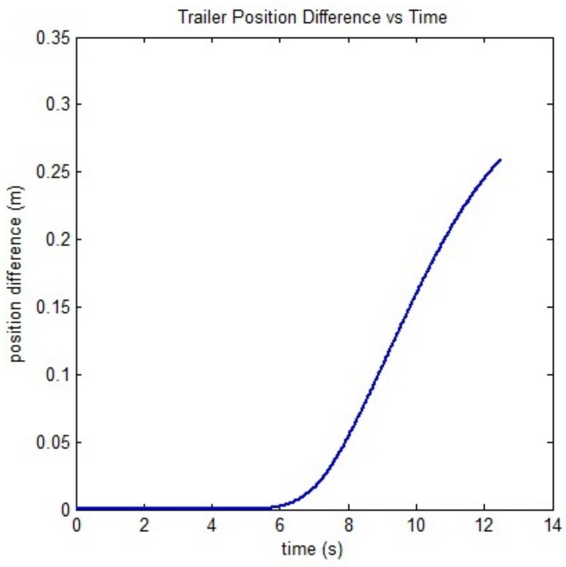

Figure 2.11: Position Differences between the Kinematic and Dynamic Models

2.4 Conclusion

This chapter presented two models, a kinematic model and a dynamic model, which could be used in the design of an MPC controller. The kinematic model takes significantly less computation effort, but the dynamic model is more realistic in that it considers the momentum of the vehicles, and it acknowledges that the tires have slip. The slight difference in the outputs of these two models allows for the testing of an MPC controller's ability to compensate for model error before physically implementing the control system on a robot.

Chapter 3

Applying MPC to a Tractor Trailer System

This chapter describes the Model Predictive Control (MPC) algorithm used to control the tractor-trailer system. First, a front-wheel steering tractor model is considered, followed by a skid-steering vehicle. MPC follows two key steps: set point calculations, and control calculations. To test these control methods, an S-curve path was designed with two 5-meter radius turnarounds as shown in Figure 3.1.

3.1 Set Point Calculations

When learning to drive a motor vehicle, a human driver gradually gains some idea of how the vehicle will respond to a certain steering input. When preparing to make a turn at a traffic light (particularly left turns), the driving instructor tells the new driver to visualize an arc from the vehicle's current position to where the vehicle will be after making the turn. When the light turns green, the driver follows the arc, anticipating the car's response to a steering input by using preexisting knowledge of the vehicle's response from previous turns. In the MPC algorithm, the same principle is applied using a model to predict the outcome, given a steering input.

Figure 3.2 on page 28 illustrates the steps taken for the set point calculations. Subscript k indexes how many cycles the set-point calculator has run, while subscript i tracks the number of guesses the computer has made during its current prediction cycle. Every time the algorithm recycles, the current position and heading of both the tractor and trailer are accounted for, and an initial guess is made by using the previous tractor steer angle. The algorithm then uses the model to predict the path the trailer would follow over next 4 seconds. Next, using the desired path as a reference, a cost function is calculated based on how far

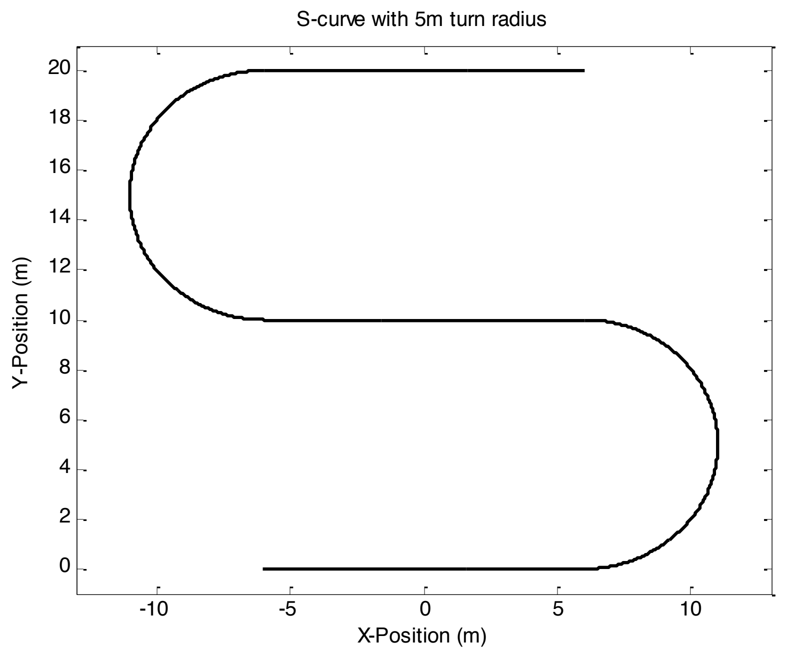

Figure 3.1: Simulation Path

the predicted path is from the desired path. If this is the first iteration of the prediction cycle, the steer angle is moved 1° in the direction of the path, and the process is repeated to calculate another cost value. On subsequent iterations, Newton's Method is applied in an effort to bring the cost as close to zero as considered reasonable. Once a steering angle has been determined that minimizes cost, that steer angle is sent to the steering controller as a reference.

3.1.1 Initial Setup

At the start of the prediction cycle, the algorithm receives position and heading information from a GPS receiver attached to the trailer (X_k,Y_k, θ_k). If the tractor is a front-steering vehicle, the algorithm also takes the current steer angle (δ_k) from a wheel encoder attached to the steering wheel. On the other hand, if the tractor is a skid-steering vehicle, the algorithm notes the current angular velocity of the tractor. The algorithm also assumes a constant forward velocity (v) of the tractor. For the first prediction, the algorithm uses the

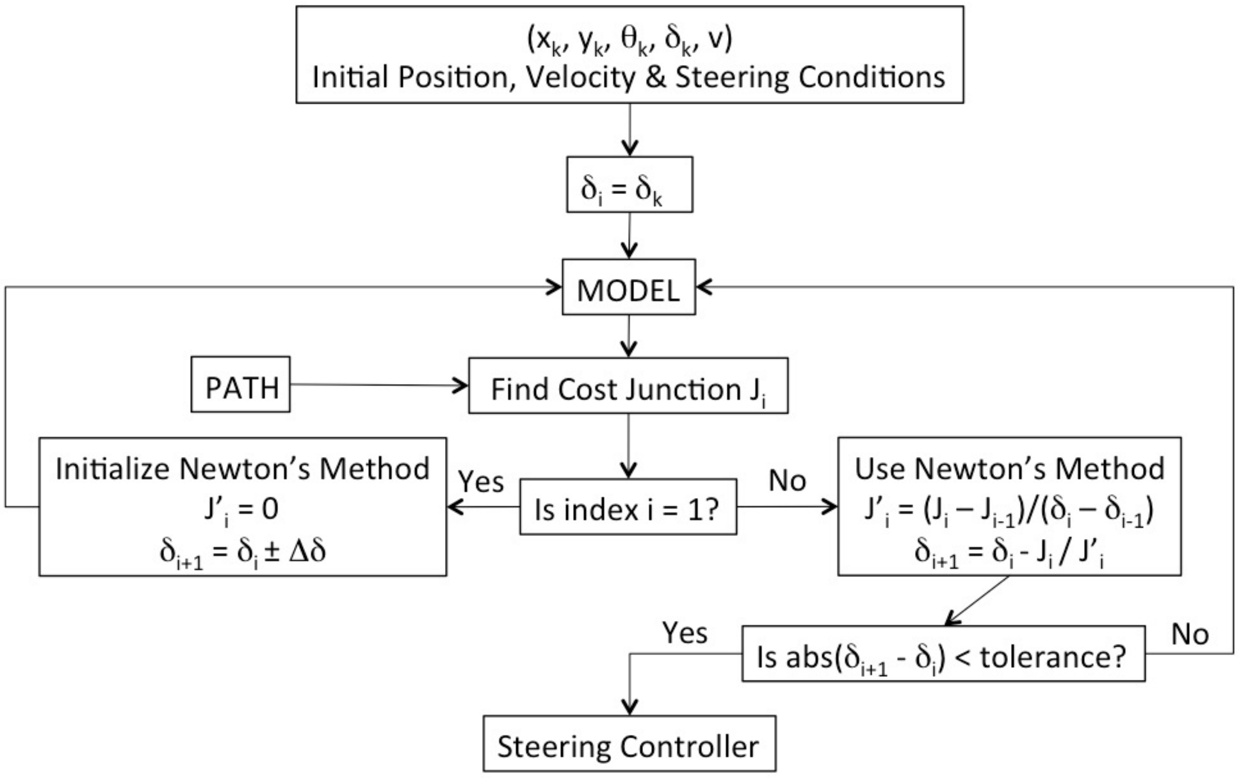
$(x_k, y_k, \theta_k, \delta_k, v)$
Initial Position, Velocity & Steering Conditions
$\delta_i = \delta_k$
MODEL
PATH
Find Cost Junction J_i
Initialize Newton's Method
$J'_i = 0$
$\delta_{i+1} = \delta_i \pm \Delta\delta$
Yes
Is index i = 1?
No
Use Newton's Method
$J'_i = (J_i - J_{i-1})/(\delta_i - \delta_{i-1})$
$\delta_{i+1} = \delta_i - J_i / J'_i$
Yes
Is $\mathrm{abs}(\delta_{i+1} - \delta_i)$ < tolerance?
No
Steering Controller

Figure 3.2: Set Point Calculations Flowchart

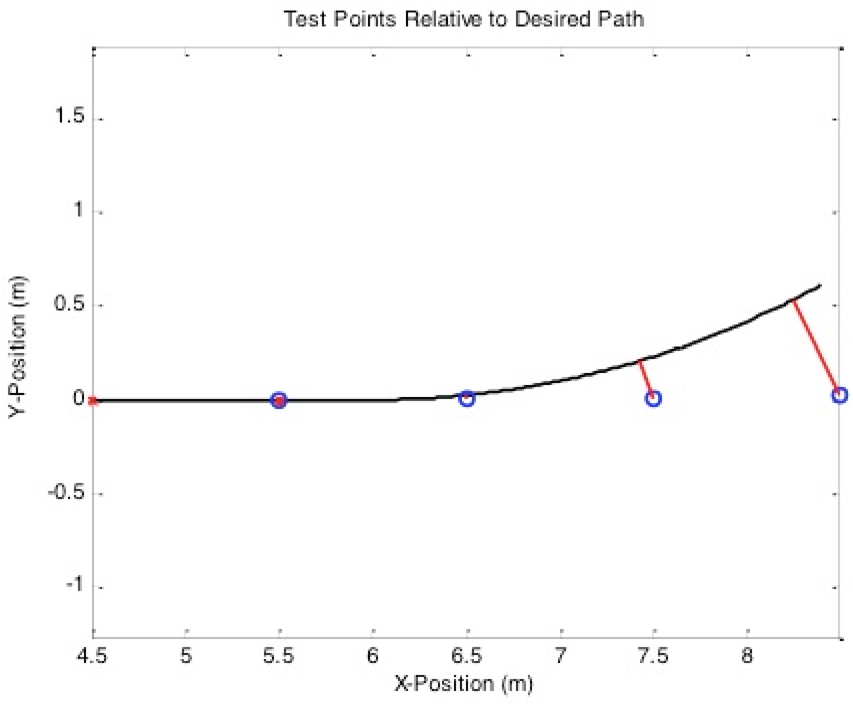

Figure 3.3: Test Points Relative to Desired Path

current steering angle and the model to predict the path the trailer would take over the next 4 seconds using that same steering angle.

Figure 3.3 shows an overhead view of this happening. The trailer is located on the left of the plot, the black line is the intended path, the blue circles indicate the trailer's predicted locations – one meter apart from each other, and the red lines indicate the distance between each prediction point and the path.

Now, to find the optimal steer angle, a cost function is defined. Ordinarily, the MPC cost function takes the form shown in Equation (3.1).

$$J = \sum_{j=1}^{N} \left[Q_j \left(r_j - x_j \right)^2 + R_j \Delta u_j^2 \right] \tag{3.1}$$

When using linear MPC, the analytical algorithm shown in Appendix A can be used to calculate the control input. In the case of a nonlinear approach, iterative methods have to be applied. In many cases, nonlinear MPC is infeasible to implement in real time, but this research explores a way to reach an input decision quickly.

The cost function is first redefined as the sum of the distances between predicted position estimates and the path:

$$J_i = \left| \sum_{j=1}^{4} l_j (\pm 1)_j \right| \tag{3.2}$$

where l_j is the shortest distance between the j-th prediction point and the path. To ensure that this summation converges to zero, all test points to the right of the path are assigned a positive value, while the test points to the left are assigned a negative value.

Notice that the cost function defined by Equation (3.2) is no longer quadratic, and instead it has been surrounded by absolute value brackets. Without the absolute value brackets, the summation could go negative if all prediction points were on the left side of the path, and a negative cost would imply the existence of a steer input better than optimal. The absolute value brackets simply state that the length summations that go negative are just as unfavorable as positive summations.

To determine what the sign should be for each point, some trigonometry is used. First, the algorithm determines for each point, what angle the path makes with the trailer's heading and the nearest point on the path: $\theta_{path_j} = \arctan\left(\frac{Y_{path_j} - Y_{trailer_k}}{X_{path_j} - X_{trailer_k}}\right)$. The algorithm then determines the angle that the prediction point makes with the trailer's current heading: $\theta_{pred_j} = \arctan\left(\frac{Y_{trailer_j} - Y_{trailer_k}}{X_{trailer_j} - X_{trailer_k}}\right)$. After that, it compares these two angles, and it assigns a cost function value: $J_i = \left|\sum_{j=1}^{4} l_j \cdot \text{sign}\left(\theta_{path_j} - \theta_{pred_j}\right)\right|$.

It is fair to ask a few questions at this point, starting with "Why go to all this effort?" The reason is that this ensures (in most cases) that the interior of the cost function crosses zero on the y-axis of a cost versus steer angle plot. This sets things up nicely for using Newton's Method to find the zero of the cost function quickly and efficiently. It is important to point out that this cost function will not return the same solution as Equation (3.1), but the horizon can be adjusted to mimic the solution of (3.1) by heavily weighing the later predictions.

The follow-up question would then be, “Why not just use the derivative form of Newton’s Method to minimize the cost function in Equation (3.1)?” The problem is that each iteration of the derivative form of Newton’s Method requires at least two cost evaluations to compute a derivative. This doubles the computational expense of the minimization process. If the robot’s processor is fast enough to compute these calculations in real time, using (3.1) might be feasible, but if the processor cannot keep up, unpredictable results would occur.

There are two pitfalls to this redefined cost function, however. One being that there could potentially be more than one solution to the cost function on any given point on the path. First, there is the desired solution that keeps the system moving along the path toward the goal. Then, there may be another solution where the tractor is spinning at a dangerously high turn rate, but the kinematic model evaluation shows that the sum of the trailer’s position predictions still add up to zero. This is especially prevalent on a skid-steer robot, as the distance between the tractor’s center of rotation and the hitch is long, and a sharp turn causes the trailer to yaw in the other direction for a brief moment. On the other hand, a front-steer robot is less likely to have that problem as its center of rotation is the back axle, and the distance from the back axle to the hitch is relatively short compared to the rest of the vehicle.

Another pitfall is that if the robot drifts too far away from the path, the robot could reach a position and heading where no steering input exists which would allow the cost function to reach zero. Although it is tempting to use the derivative form of Newton’s Method to find the minimum in these cases, simulator tests have shown that the derivative form of Newton’s Method could inadvertently converge onto the *maximum* of the cost function, not the minimum. The fallback method in both of these situations is Golden Section Search, which while inefficient, guarantees that the solution is a minimum, and it limits the search range to a user-defined interval.

3.1.2 Finding Minimum Cost Using Newton's Method

Finding the minimum cost is a trial-and-error process, but a good initial guess is the same steer angle used for the previous prediction cycle. The algorithm uses this guess along with the model to predict where the tractor and trailer would go. Then, the second guess is 1° to the right or left of that angle (depending on which side of the initial guess the path is on). With two points available, the algorithm can now predict a third point using Equations (3.3) and (3.4).

$$J_i' = \frac{J_i - J_{i-1}}{\delta_i - \delta_{i-1}} \tag{3.3}$$

$$\delta_{i+1} = \delta_i - \frac{J_i}{J_i'} \tag{3.4}$$

Figure 3.4 on page 33 illustrates the Newton's Method process. Each frame in Figure 3.4 depicts the results of a prediction. On the top subplot of each frame, the trailer GPS receiver is located on the far left-hand side of the plot. The black line is the path. The blue circles are prediction points based off of the model, one second apart from each other. The red lines represent the distance from each point to the path. On the bottom subplot of each frame, the x-axis is the steering angle, while the y-axis is the cost. The blue line is the cost function that occurs under the current tractor-trailer state conditions, which was computed only for this demonstration, but is impractical to compute in real time. Finally, the red line tracks each prediction made using Newton's Method.

The cycle repeats itself until the change in steer angle is less than 0.5°. As seen in the Figure, the prediction algorithm ran five times to arrive at the steering angle with a cost near zero. By reusing the previously calculated steering angle, however, the algorithm usually arrives at a usable steering angle after three predictions. Figure 3.5 on page 34 shows an overhead simulation of the system guiding to the path using this MPC approach, assuming the controller could guide to the set points instantaneously.

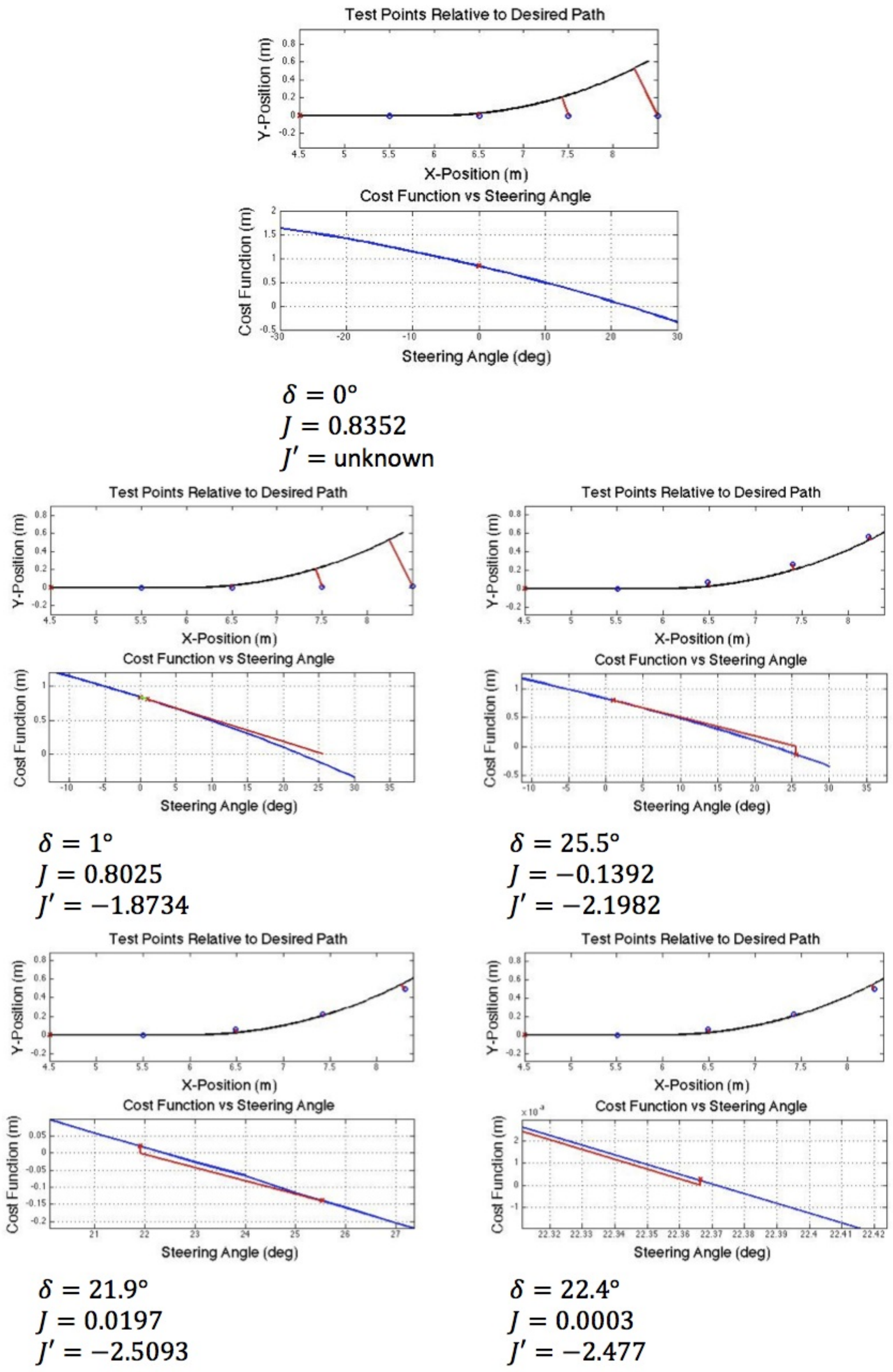

Figure 3.4: Newton's Method Demonstration

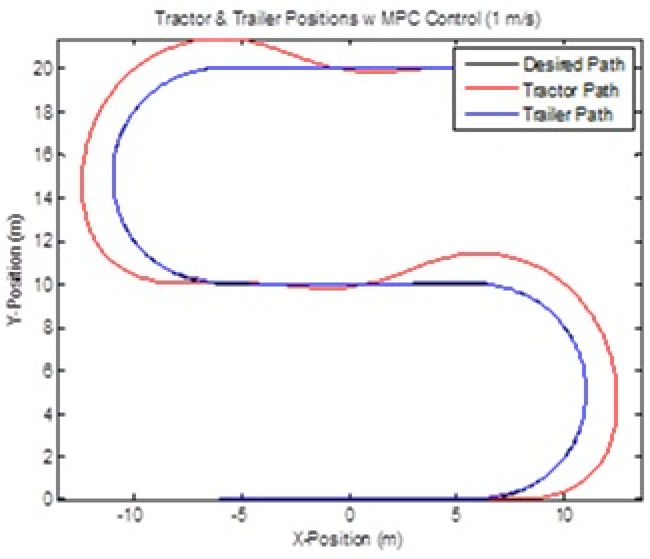

Figure 3.5: MPC Set Point Simulation

If the tractor vehicle is a skid-steer vehicle, such as the Segway RMP 400, the controller uses the same prediction method as before, but it chooses the necessary turn rate (instead of the steer angle) in order to keep the trailer on the path.

3.1.3 Finding Minimum Cost using Golden Section Search

In some cases, the Newton's Method approach will not work, as the cost function does not cross zero on the y-axis. This is especially likely to happen with tractor-trailer systems where the distance between the center of rotation on the tractor and the hitch is long. It can also happen when the path following error exceeds a certain point. Figure 3.6 shows an instance where using MPC on a Segway RMP 400 and trailer system, the cost function would not reach zero, no matter what steering input is used. To address this, the cost function is first squared to eliminate the possibility of it going negative, and the Golden Section Search method of optimization is used.

Again, it is tempting to try the derivative form of Newton's Method to locate the minimum, but in some cases, a local minimum and local maximum are very close together. This could result in Newton's Method converging onto a local maximum. Once this happens, the

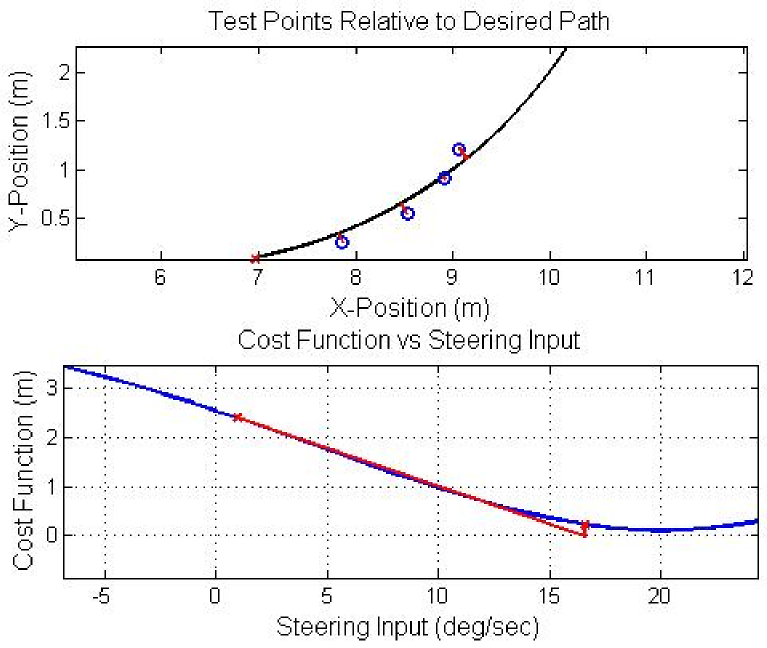

Figure 3.6: Newton's Method Incompatibility

robot continues to follow this method, maintaining its steering input on the local maximum of the cost function and loses the path completely. On the other hand, the Golden Section Search method guarantees a minimum, provided that a local minimum exists on the chosen interval.[16]

The prediction points for the Golden Section search method are chosen the following way. First a prediction interval is chosen (in the case of the Segway, -40 deg/sec to 40 deg/sec). If l_0 defines the length of the full interval, and l_1 and l_2 define the space between the left and right edges of the interval and the intermediate prediction points, the locations of l_1 and l_2 can be determined by satisfying the following conditions:

$$l_1 + l_2 = l_0 \tag{3.5}$$

$$\frac{l_1}{l_0} = \frac{l_2}{l_1} \tag{3.6}$$

By substituting Equation (3.5) into Equation (3.6), the following equation results:

$$\frac{l_1}{l_1 + l_2} = \frac{l_2}{l_1} \tag{3.7}$$

Next, the reciprocal is taken, and R is defined as $\frac{l_2}{l_1}$, resulting in the following:

$$1 + R = \frac{1}{R} \tag{3.8}$$

By multiplying both sides by R, Equation (3.8) becomes $R^2+R-1 = 0$, and the positive root, or the *golden ratio* can be solved for. The result is $R = \frac{\sqrt{5}-1}{2} \approx 0.61803$.

To set up the algorithm, x_l and x_u define steer inputs at the lower and upper limits of the prediction interval. The intermediate points x_1 and x_2 are then chosen using the golden ratio:

$$x_1 = x_l + \frac{\sqrt{5}-1}{2}(x_u - x_l) \tag{3.9}$$

$$x_2 = x_u - \frac{\sqrt{5}-1}{2}(x_u - x_l) \tag{3.10}$$

The costs of these two intermediate points are then evaluated and a comparison is made. Figure 3.7 illustrates this process. In the cost function presented, $J(x_2) < J(x_1)$, so all steer inputs greater than x_1 are eliminated, and x_1 becomes x_u for the second iteration. Also, thanks to the use of the golden ratio, the new x_1 lies at the same point as the old x_2, so the cost of that point has already been evaluated and can be reused for the second iteration. The new x_2 is found by again using Equation (3.10), and its associated cost is evaluated. This time, $J(x_1) < J(x_2)$, so all steer inputs less than x_2 are eliminated, x_2 becomes the next x_l, and x_1 becomes the next x_2. After 10 repetitions, the interval shrinks to about 0.8% of its original size, giving a turn rate that is accurate to within 0.64 degrees per second.

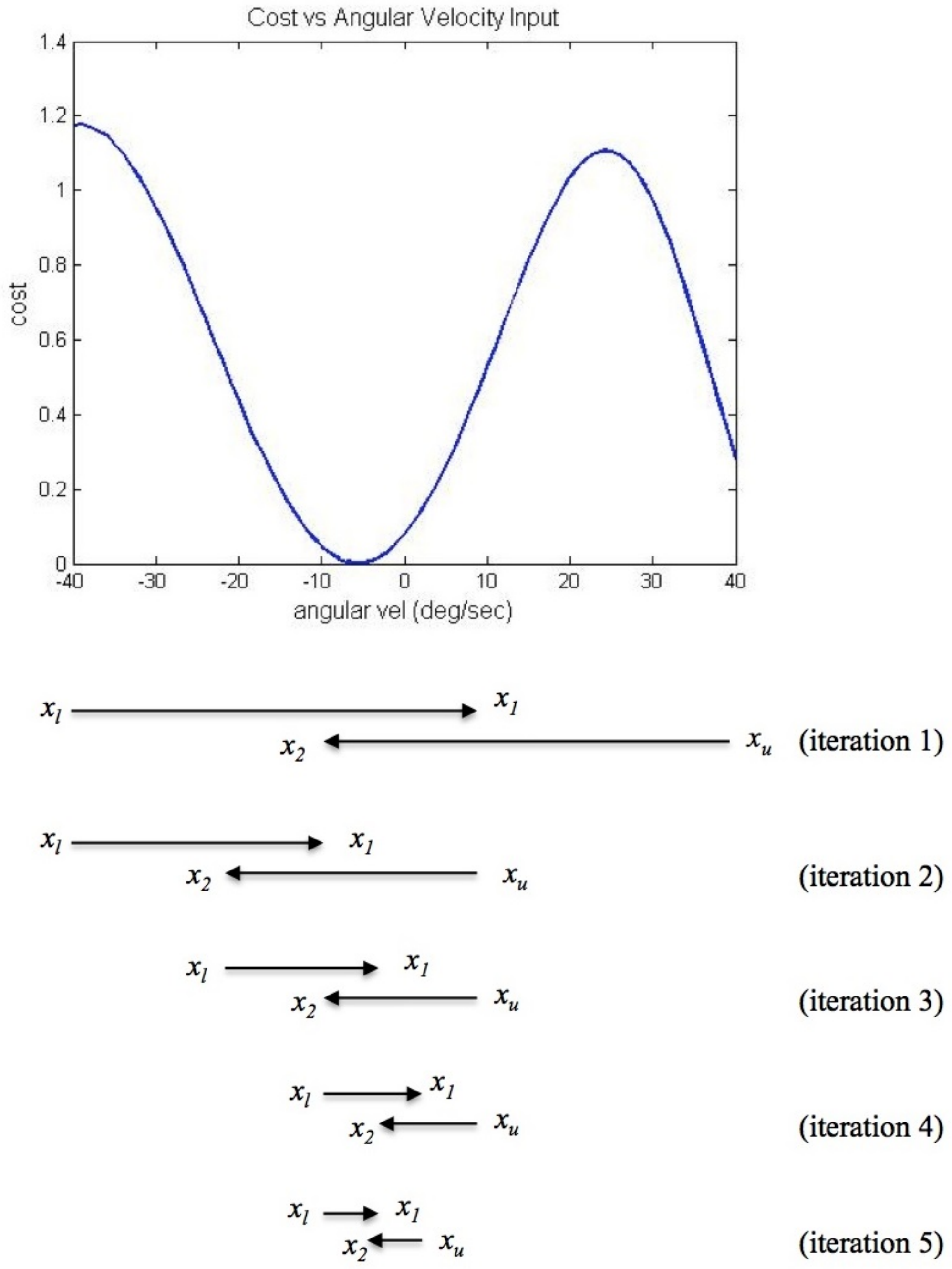

Figure 3.7: Golden Section Search

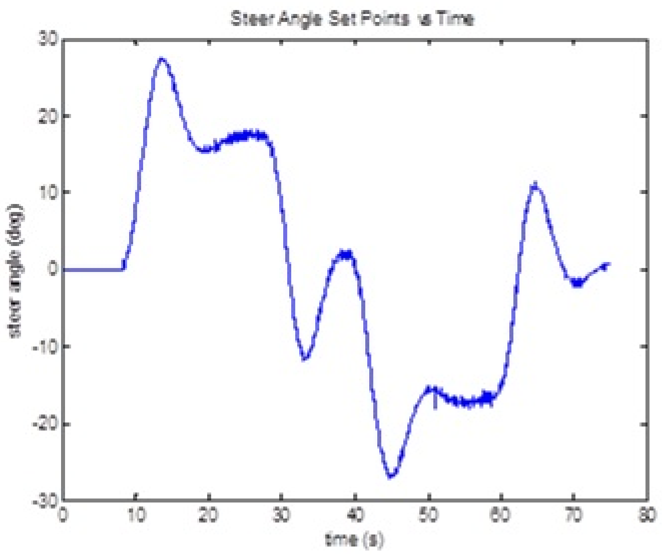

Figure 3.8: Steering Angle Set-Points

3.2 Control Calculations

Once the steering angle has been decided, the controller uses this steering angle as a reference angle and uses a PID algorithm to determine the voltage to the motor to achieve that angle quickly. For the Segway, instead of using Equation (2.1) to determine a steer angle and compute the corresponding turn rate, the turn rate is decided directly during the set point calculations. Then, the Segway's computer makes the control calculations internally to achieve that turn rate. What follows in this section is a method to design a controller to determine the voltage for a steering motor on an Ackerman-steered vehicle.

3.2.1 Steering Motor Voltage Calculations for Front-Steering Tractor

Looking at Figure 3.8, there are noticeable abrupt changes in the steering angle. The goal of the control calculations is to not only determine a voltage to apply across the motor, but to also smoothen out the rough spots on the set point plot.

Figure 3.9 shows a block diagram for an armature motor. This model has the closed-loop transfer function:

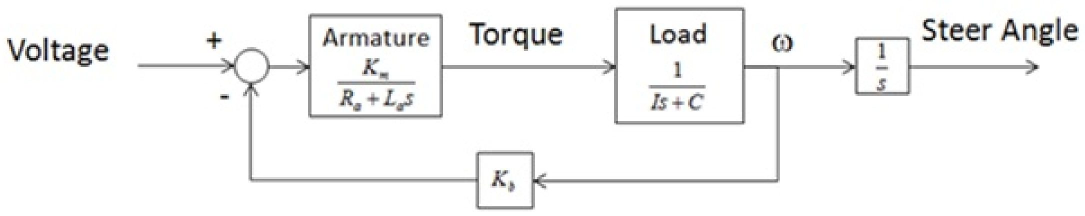

Figure 3.9: Armature Motor Model

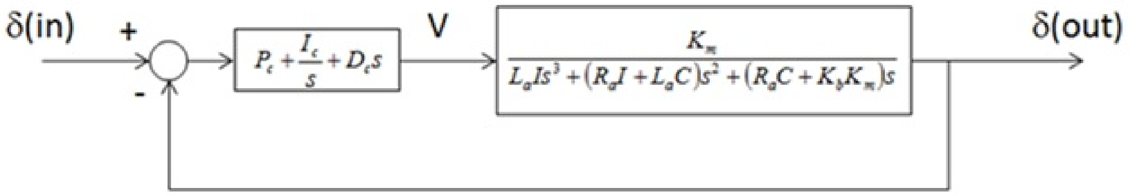
δ(in)
+
-
$P_c + \frac{I_c}{s} + D_c s$
V
$\frac{K_m}{L_a I s^3 + (R_a I + L_a C)s^2 + (R_a C + K_b K_m)s}$
δ(out)

Figure 3.10: Controlled Motor System

$$\frac{\delta(s)}{V(s)} = \frac{K_m}{s\left[(L_a s + R_a)(Is + C) + K_b K_m\right]} \tag{3.11}$$

For the simulations done in this thesis, the following parameters were used for the motor:

$R_a = 1\Omega$

$L_a = 0.001H$

$K_b = K_m = 0.05Vs/rad$

$I = 0.0035kg\ m^2$

$C = 0.1Js/rad$

If a PID controller were applied, the closed-loop system would take the form shown in Figure 3.10. The following is the complete closed-loop transfer function for the controlled system:

$$\frac{\delta_{out}(s)}{\delta_{in}(s)} = \frac{K_m\left(D_c s^2 + P_c s + I_c\right)}{L_a I s^4 + (R_a I + L_a C)\, s^3 + \left[(R_a C + K_b K_m) + K_m D_c\right] s^2 + K_m P_c s + K_m I_c} \tag{3.12}$$

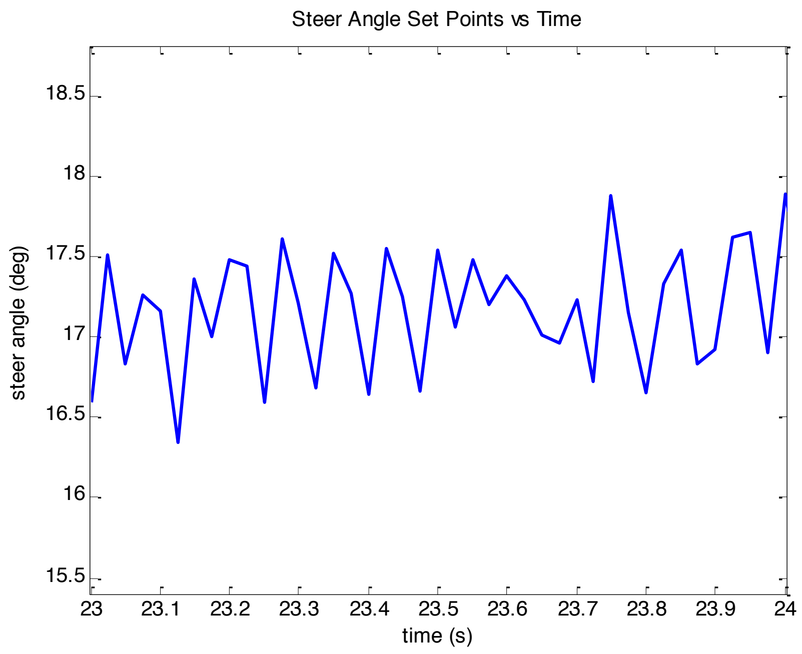

Figure 3.11: Unwanted Oscillations

The goal of this controller is to not only decide on the voltage to apply to the motor, but also to filter out unwanted oscillations. In order to choose suitable P_c, I_c, and D_c values, the unwanted oscillations were visually examined (see Figure 3.11). It is seen that the oscillation period is around 0.1 seconds, translating to a target filter frequency of about 10 Hz. Using the 'bode' command in Matlab, the frequency response of the system could be examined under a variety of PID conditions.

First, a simple proportional controller was considered with a gain of 4. This yielded a bode plot with a cutoff frequency of 0.332 Hz, and a -37.6 dB gain in the amplitude (which is an absolute amplitude of nearly zero) at 10 Hz (62.8 rad/sec). Figure 3.12 illustrates these findings.

Next, a proportional-integral controller was considered with a P_c gain of 3, and an I_c gain of 6. This changed the cutoff frequency to 0.501 Hz, and the 10 Hz oscillation amplitude to -40.1 dB (see Figure 3.13).

The PI controller appears to work in simulation, but these results are misleading. As seen in Figure 3.14, the steering angle movements are now smooth. However, Figure 3.15

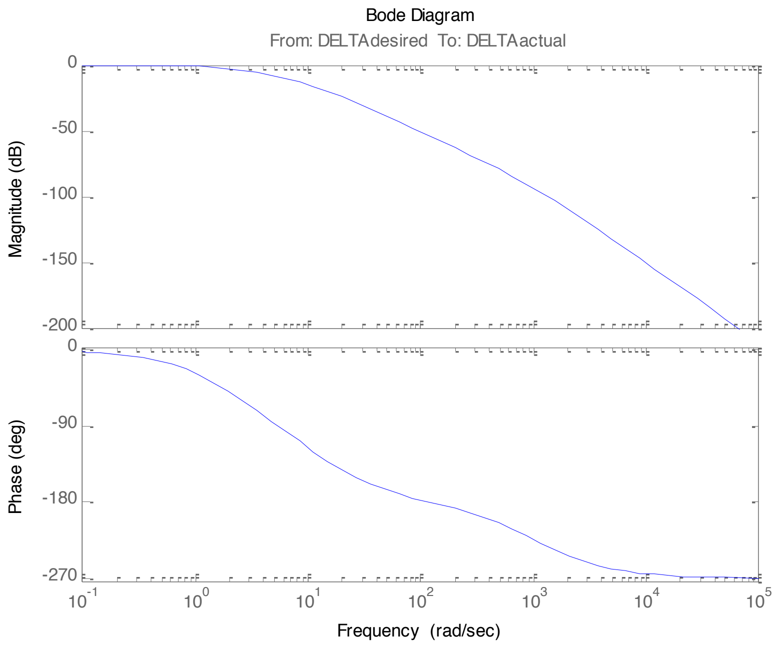

Figure 3.12: Proportional Control

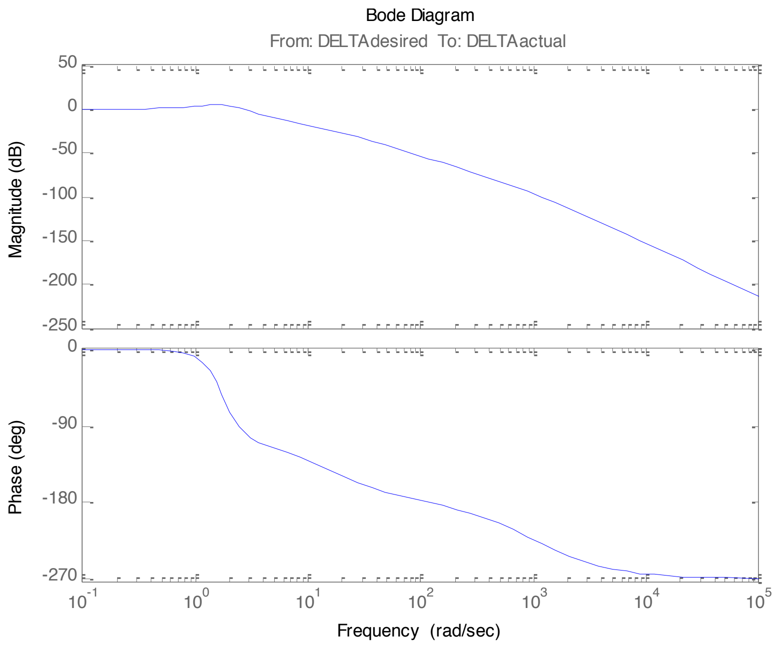

Figure 3.13: Proportional-Integral Control

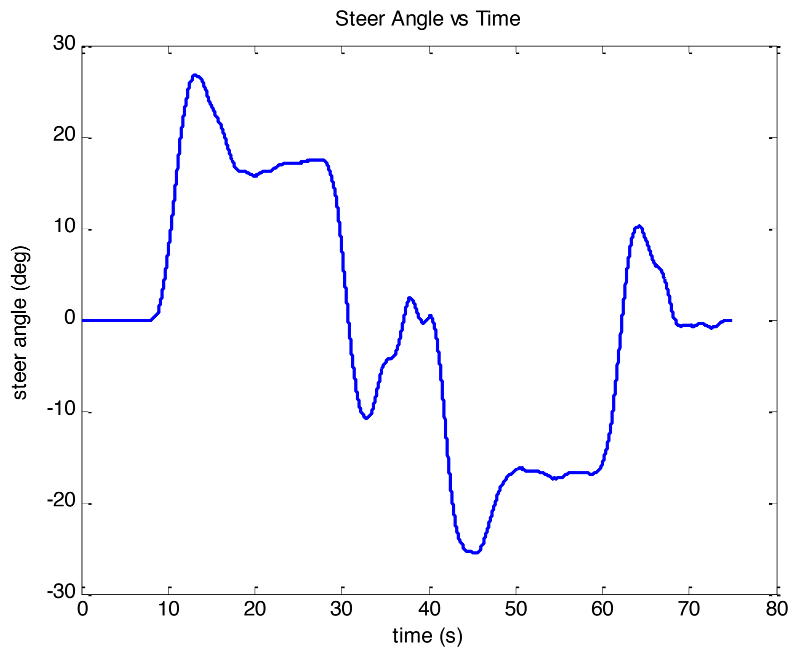

Figure 3.14: Steer Angle Controlled

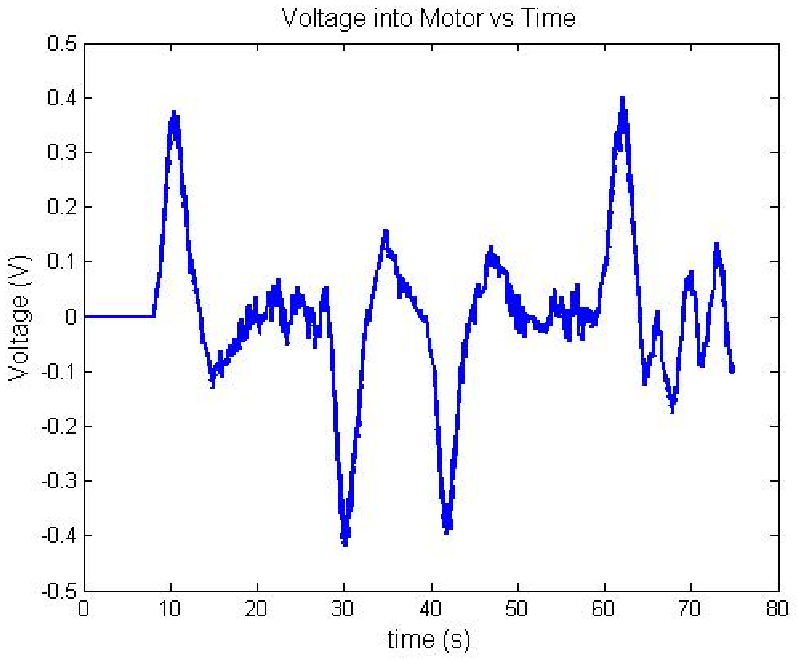

Figure 3.15: Voltage Across Motor vs Time (using PI control)

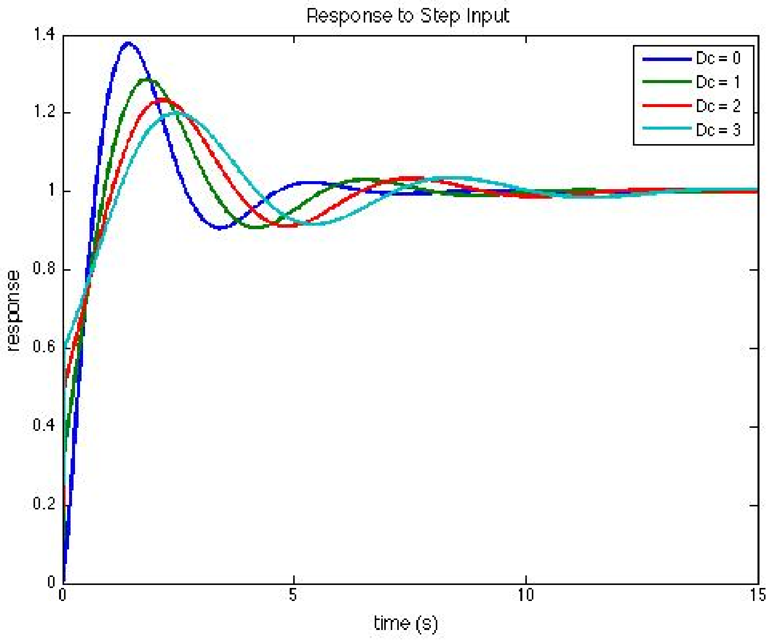

Figure 3.16: Motor Response to Step Input with Varying Derivative Control Values

shows rapid voltage changes. It is physically impossible for a controller to adjust that quickly, so a PID controller is employed.

When considering a response to a step input, a small latency introduced by the PI controller is desired since it filters away the unwanted oscillations, and thus, a PID controller that carries a similar latency is desired. In Figure 3.16, the step response of the controlled motor is examined under the same proportional and integral gains ($P_c = 3$, $I_c = 6$), and different derivative control gains. As D_c is increased, the latency increases, and the overshoot drops. Ultimately, the gains $P_c = 3$, $I_c = 6$, and $D_c = 2$ were chosen. Figure 3.17 shows the resulting voltage.

3.3 Conclusion

This chapter described the prediction – control method used in the guidance of a robot-trailer system. The algorithm first chooses a steering angle, then it predicts where the trailer would go over the next four seconds using that steering angle, and finally it calculates

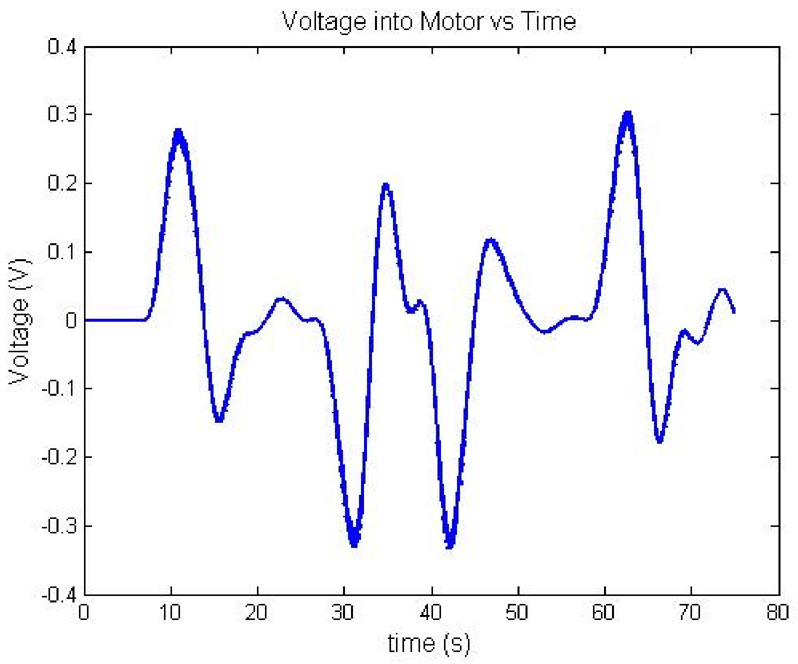

Figure 3.17: Voltage Across Motor vs Time (using PID control)

a cost based on how far the trailer's predicted movement deviates from the path over that time. This process is repeated, using a Newton's Method & Golden Section Search hybrid algorithm to force the steering angle to converge on the "optimal" steering angle. If the robot is a skid-steer vehicle, the controller determines the required turn rate for the robot in radians per second in lieu of the steering angle. From there, control calculations can be made in order for the robot to achieve the desired steer angle or turn rate.

Chapter 4
Computer Simulations and Live Application

This chapter presents the observations made by running various computer simulations, as well as a live application, using this controller. First, since this control system was originally intended to be used on an Ackerman-steered vehicle, the controller's performance was examined against a bicycle model under varying turn radii. Next, a simulation was done using a real-time simulator for a differential-steered robot. Finally, this controller was uploaded onto a Segway RMP 400 robot and examined.

4.1 Kubota RTV Simulation Results

Although the hardware for the Kubota RTV is still being assembled at the time of this thesis writing, it is still possible to simulate how the controller will behave when the plant's response to an input does not match the model's prediction exactly. For the first simulation, the MPC simulator is modified to use the kinematic model to generate predictions and determine inputs, and then use the dynamic bicycle model to simulate the Kubota's response. For the second simulation, the MPC simulator uses the linearized kinematic model to generate predictions, and then it uses the nonlinear kinematic model to simulate Kubota's response.

4.1.1 Kinematic Controller Model against Bicycle Plant Model

As expected, when the controller model does not match reality, the controller is subject to significant error. Figure 4.1 shows an overhead view of the tractor-trailer path following under these conditions, while Figure 4.2 shows the error. The straight, middle section of the S-curve is between 30 and 42 seconds on the time plots.

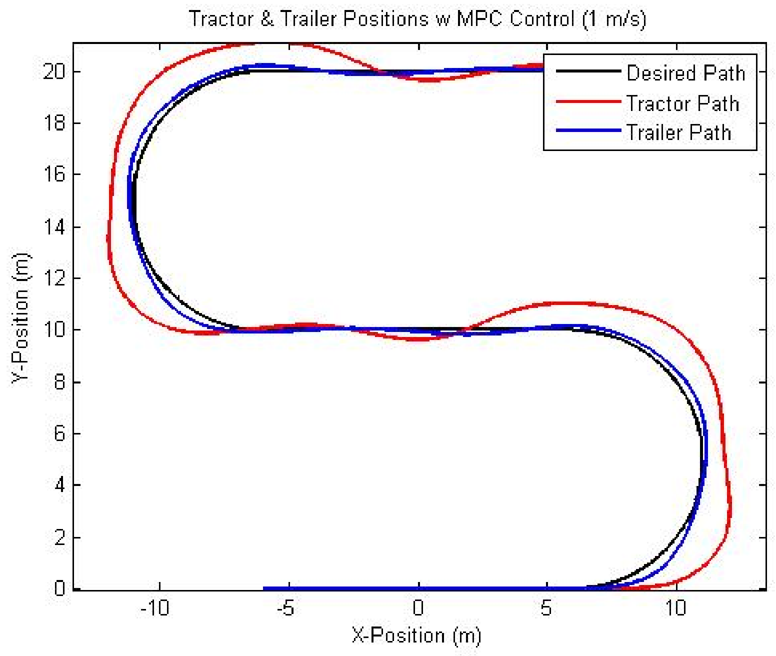

Figure 4.1: MPC with Model Error

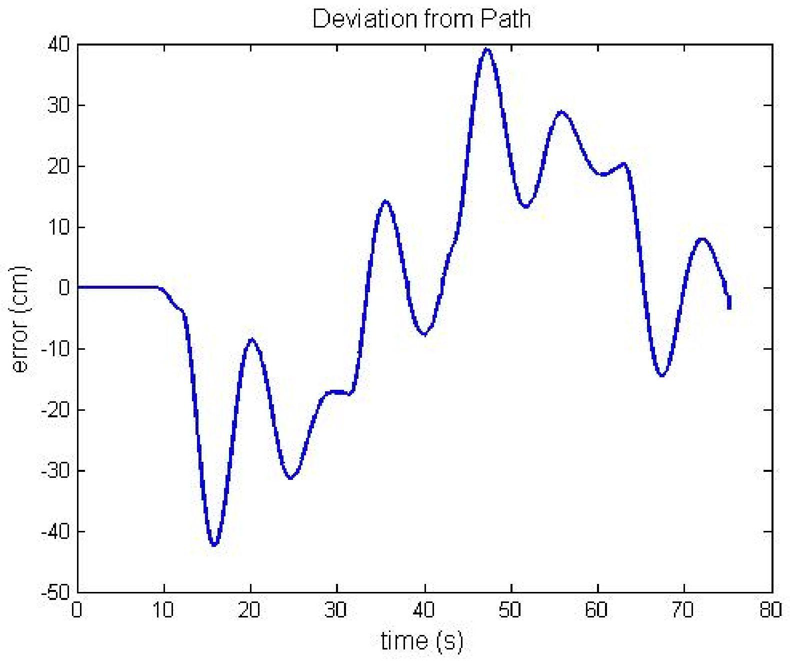

Figure 4.2: Deviation with High Model Error

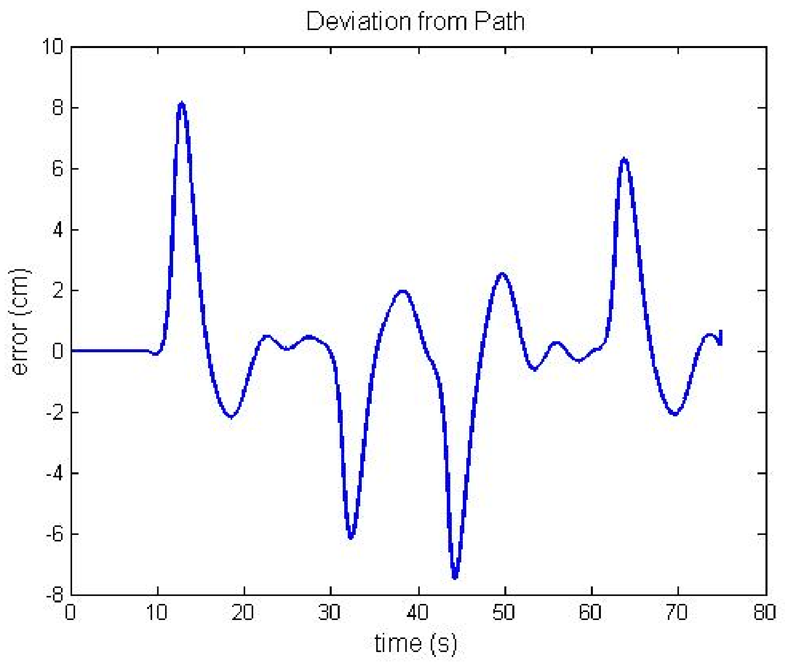

Figure 4.3: Deviation with Low Model Error

Several attempts were made to tune the controller in order to compensate for the model error. First, the prediction horizon length was varied to three seconds, five seconds, and six seconds. None of these changes reduced the maximum error. Longer prediction horizons resulted in more gradual corrections, while shorter prediction horizons caused more abrupt corrections. A prediction horizon of 4 seconds produced the least amount of error on the path turns. Second, weights were added to each prediction point (i.e. the prediction point one second ahead was multiplied by a factor of 4, the second by 3, the third by 2, and the fourth by 1). The results were similar to shortening the prediction horizon, where the tractor would turn more violently to compensate for error. In fact, weighing the earlier points by too high a factor (or having too short of a prediction horizon) would cause the tractor to veer off the path to the point of losing the path entirely and starts driving around in circles.

Conversely, a simulation was run with the kinematic model serving as the plant model as well as the prediction model. This would simulate what would happen if the model closely reflects the actual plant. Figure 4.3 shows the deviation from the path with a highly accurate

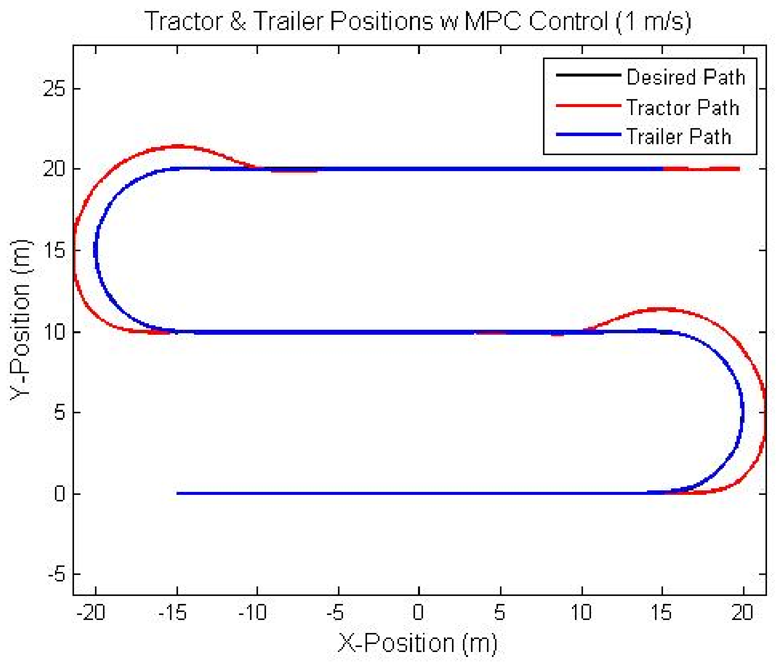

Figure 4.4: Wide S-curve Path Following

model. As seen with this model, the controller is still subject to error. The next section examines this more closely.

4.1.2 Linearized Kinematic Controller Model against Nonlinear Kinematic Plant Model

For the second simulation, the S-curve was widened so that the straight sections would be 30 meters long. This would allow for better observation of the settling time of the path following.

Figures 4.5 and 4.6 show the path following using the nonlinear and linear control models, respectively. Both models do well when following the straight sections of the path, but the nonlinear model appears to track toward the path even in the turns. In addition, since both models choose their turn rates based on future predictions, they have a tendency to make their steering adjustments early. This leads to the largest error being at the beginning and end of each turn.

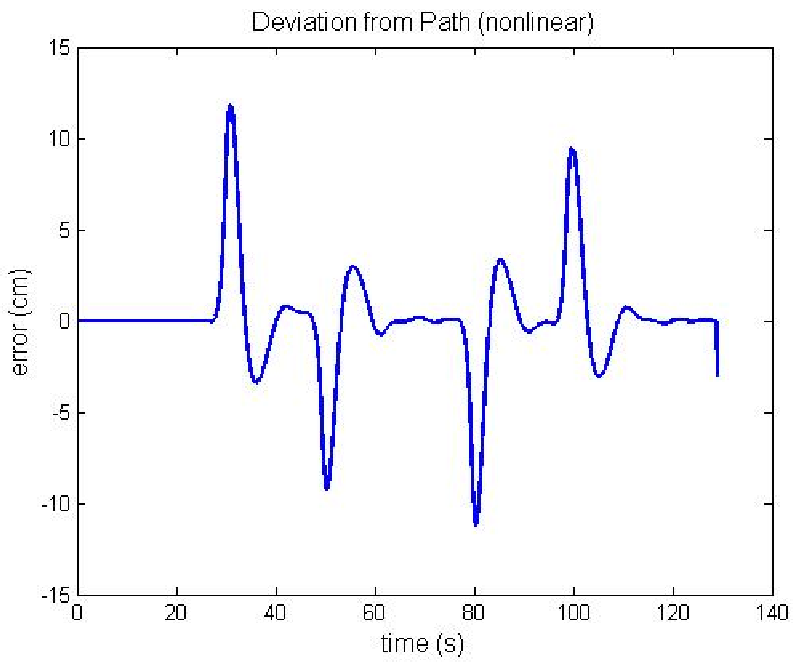

Figure 4.5: Path Following Using Nonlinear Control Model

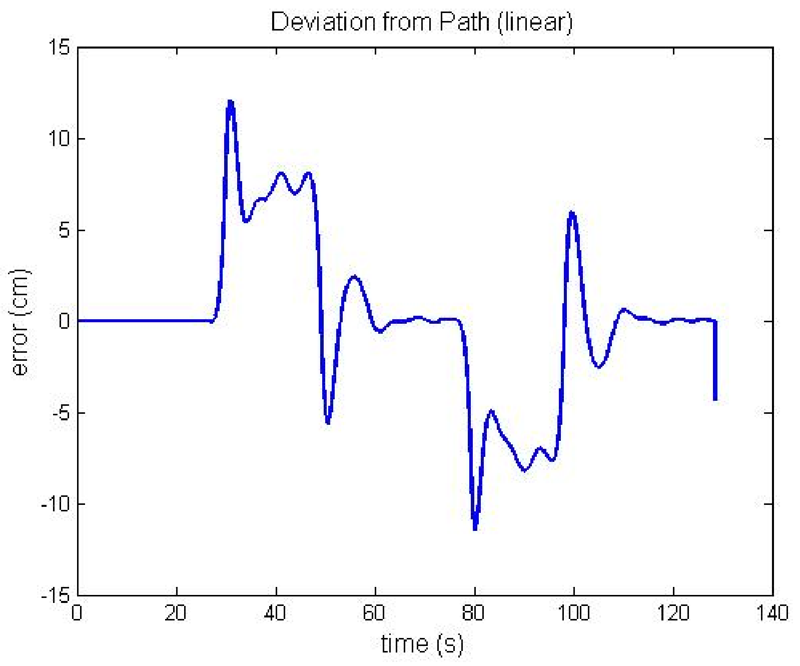

Figure 4.6: Path Following Using Linear Control Model

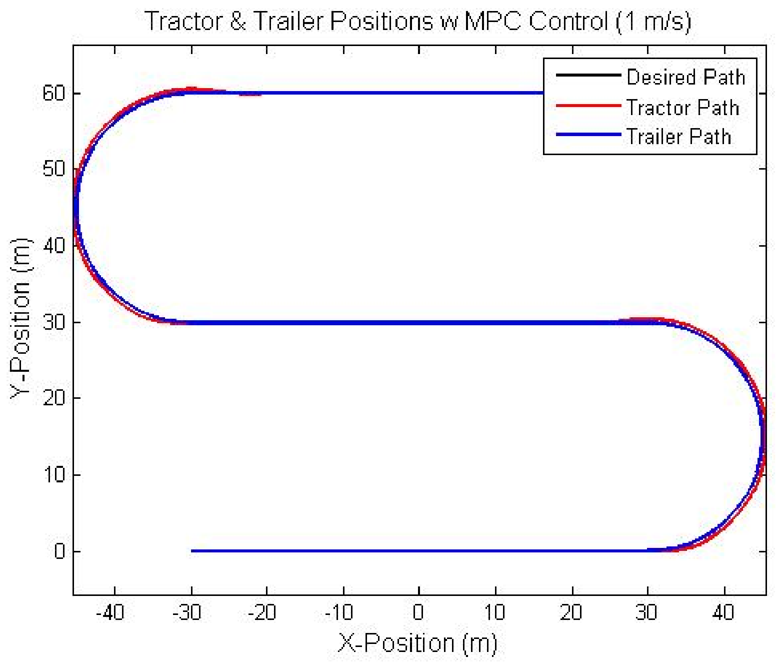

Figure 4.7: 15m Radius S-curve

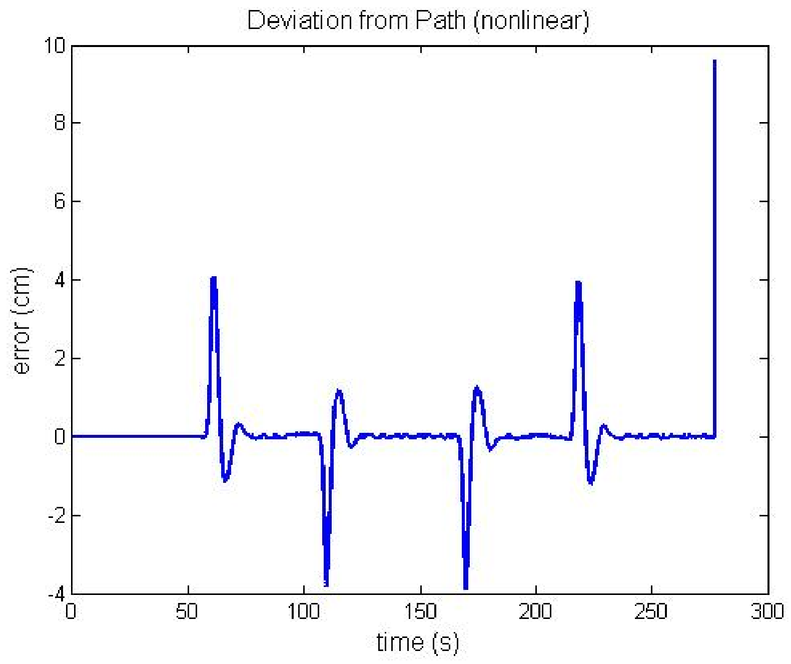

Figure 4.8: Path Following Using Nonlinear Control Model (15m radius)

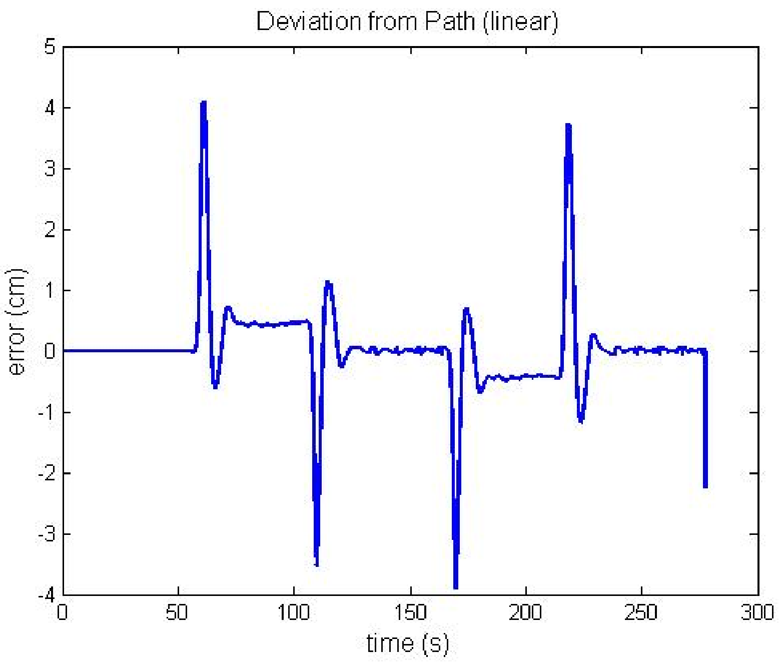

Figure 4.9: Path Following Using Linear Control Model (15m radius)

To further study this, another S-curve was made with a 15 meter turn radius. Now, steady-state error could be studied on the turns. By comparing the nonlinear controller (Figure 4.8) to the linear controller (Figure 4.9), it is seen that the nonlinear controller has a steady-state error much closer to zero than the linear controller on the turns. As seen in this simulation study, the steady-state error with the linear controller increases as the turn radius decreases, but with large turn radii, nonlinear control becomes unnecessary.

4.2 Segway Simulation Results

Next, in preparation for a live run on an autonomous vehicle, the MPC algorithm was converted from Matlab code to C++. In addition a ROS (Robot Operating System) node was written into the C++ code in order to communicate the intended control inputs to the robot. To verify that the ROS node was working properly, a test was run using the ROS node against a simulator for the Segway [18]. This simulator introduces a realistic amount

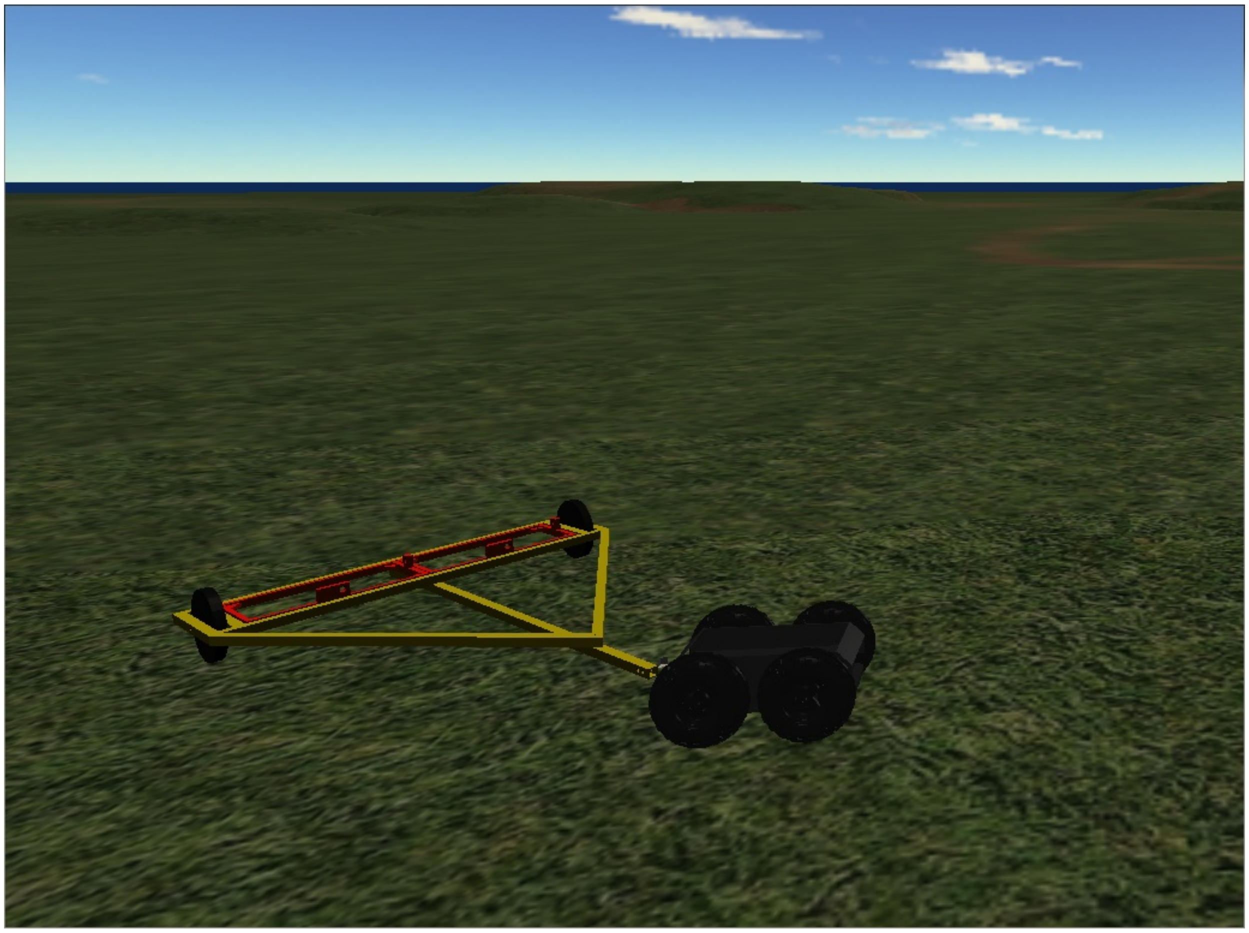

Figure 4.10: Segway Simulator [18]

of sensor noise and process noise to the feedback, allowing the testing of controller response under off-road conditions.

In order to match the Segway model used in the simulator, the control kinematic model was adjusted as shown in Table 4.1:

Parameter	Description	Value
a	Length from Tractor GPS receiver to center of front tire	0.0 m
b	Length from Tractor GPS receiver to center of back tire	0.0 m
c	Length from Tractor GPS receiver to hitch	0.56 m
d	Length from Trailer GPS receiver to hitch	2.65 m
e	Length from Trailer GPS receiver to trailer tire	0.261 m

Table 4.1: List of Segway & Trailer Simulation Parameters (kinematic model)

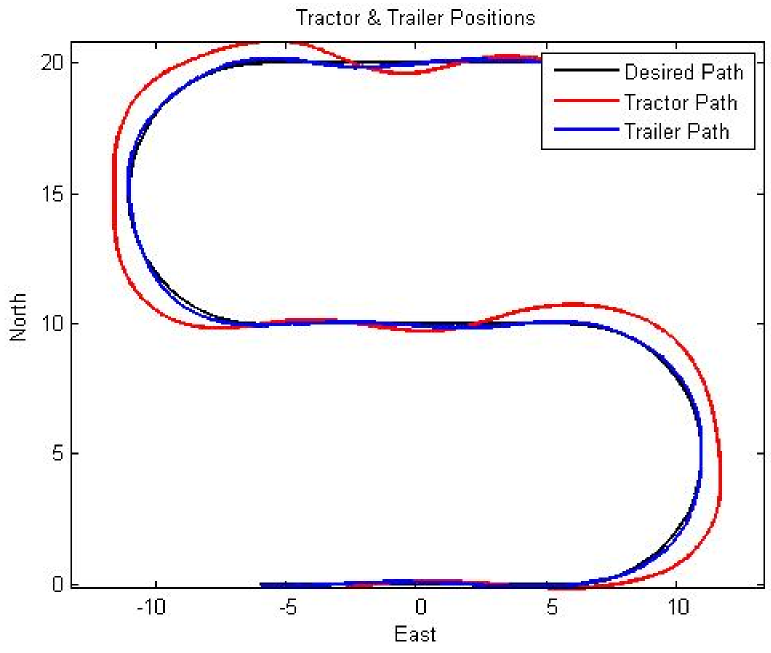

Figure 4.11: Segway & Trailer Positions, Simulated

Figures 4.11, 4.12, and 4.13 show the results from one of the runs in the simulator. As seen in Figure 4.12, the maximum error reaches about 20.8cm as the robot enters the second turn. This is due to the presence of uneven terrain and slip which were left out of the model, as well as sensor noise in the GPS measurements. With these random noise inputs, the maximum error typically ranges from 20-35cm.

The key issue to be addressed by this simulation run is to verify that the steering inputs do not reach unreasonable values. Early simulation tests with this software showed that the set points would suddenly jump to very high values, which could have potentially caused damage to the robot. This ultimately led to the inclusion of the golden section search optimization method, as it was discovered that in some cases, the cost function would not reach zero, regardless of the steering input used. As seen in Figure 4.13, the turn rate set points do not exceed 40 degrees per second. The robot first tries to zero the cost function using Newton's Method since that approach is the most efficient, but if any Newton's Method step returns a value above 40 degrees per second, the robot uses golden section search.

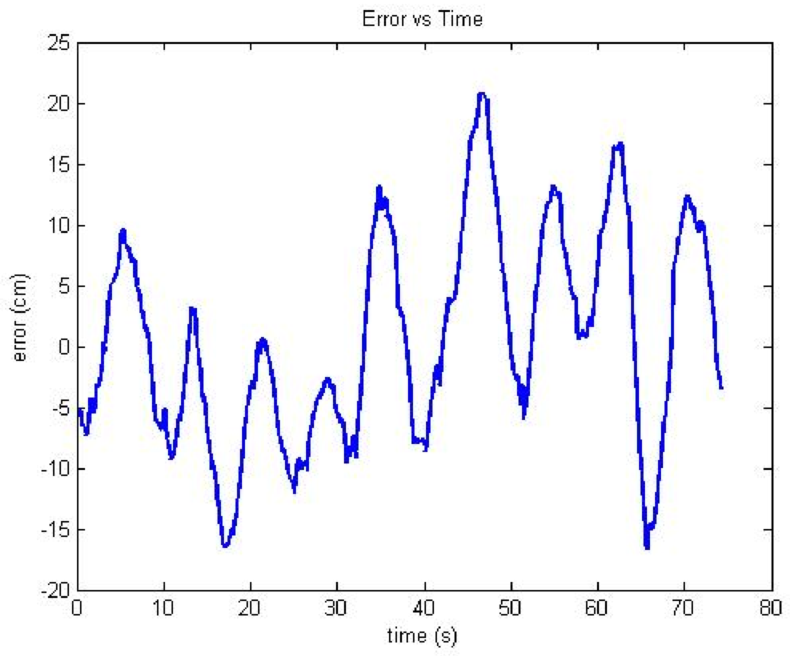

Figure 4.12: Path Following Error, Simulated

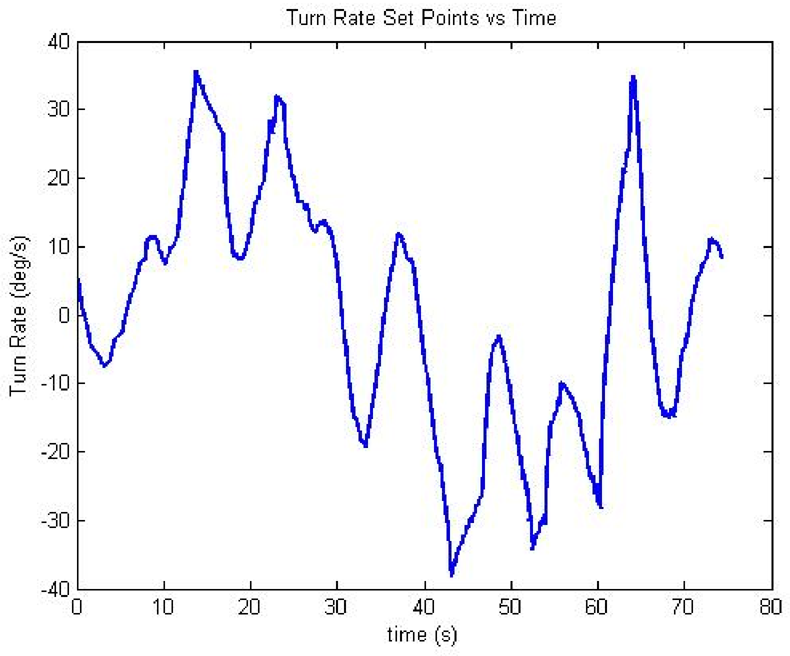

Figure 4.13: Set Points, Simulated

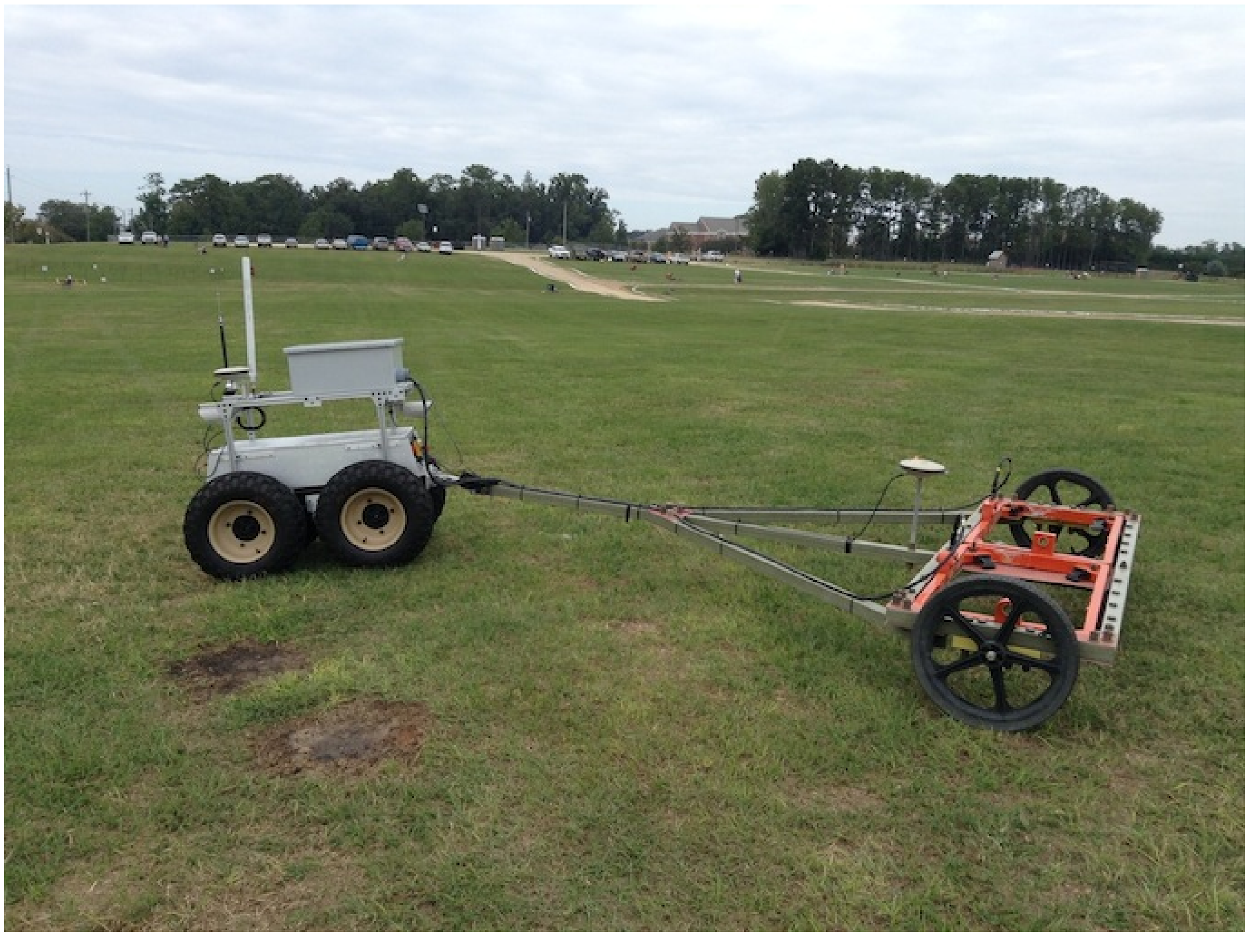

Figure 4.14: Segway Test Run

4.3 Segway Experimental Results

For the live run, the control model parameters were adjusted as shown in Table 4.2:

Parameter	Description	Value
a	Length from Tractor GPS receiver to center of front tire	0.0 m
b	Length from Tractor GPS receiver to center of back tire	0.0 m
c	Length from Tractor GPS receiver to hitch	0.615 m
d	Length from Trailer GPS receiver to hitch	2.24 m
e	Length from Trailer GPS receiver to trailer tire	0.45 m

Table 4.2: List of Segway & Trailer Live Parameters (kinematic model)

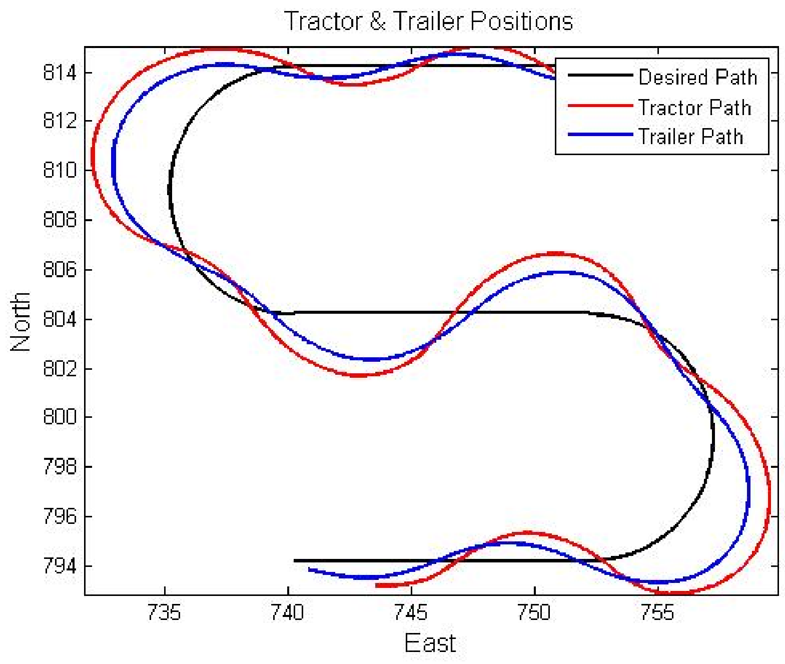

Figure 4.15: Segway & Trailer Positions (first run)

Early tests at 1 m/s reveal a sharp lag somewhere in the robot system, for reasons yet to be determined. Figure 4.15 shows an overhead view of the path following, while Figure 4.16 shows the error.

In an attempt to reduce the error, the forward speed was reduced from 1 m/s to 0.5 m/s. However as Figures 4.17 and 4.18 show, there was no significant improvement in the maximum error on the turns, but there was improvement in the path following on the straight sections of path.

Examining the set point plot of the run at 0.5 m/s (Figure 4.19), it is seen that the controller is constantly alternating between the minimum and maximum of allowable turn rates.

In addition to the control lag, another large source of error is the inconsistent traction between the Segway and the field. Often, the tires would skid against the ground, especially during the turns or going over bumps. Future tests will involve adjusting the length of the prediction horizon, adjusting the weighting on the prediction points, and allowing for faster turn rates for the Segway.

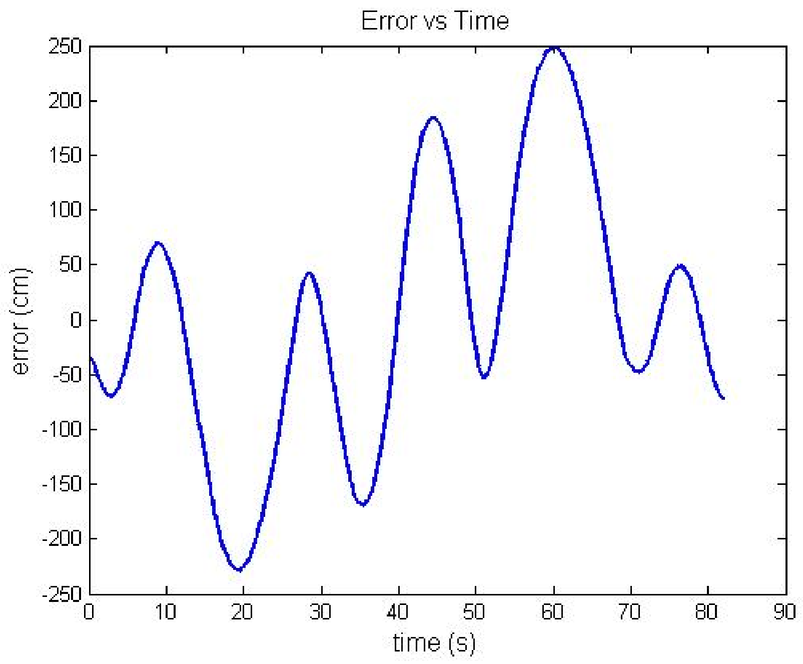

Figure 4.16: Path Following Error (first run at 1 m/s)

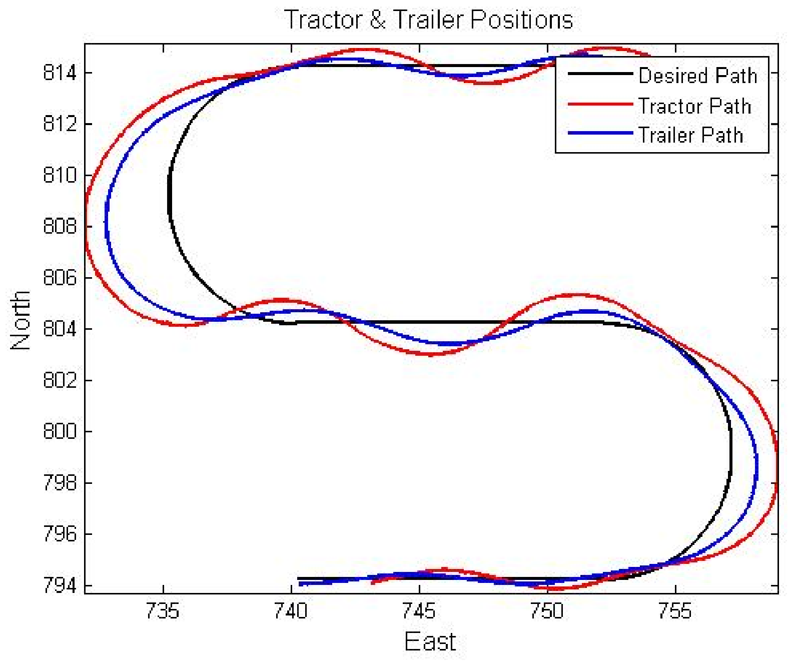

Figure 4.17: Segway & Trailer Positions (third run at 0.5 m/s)

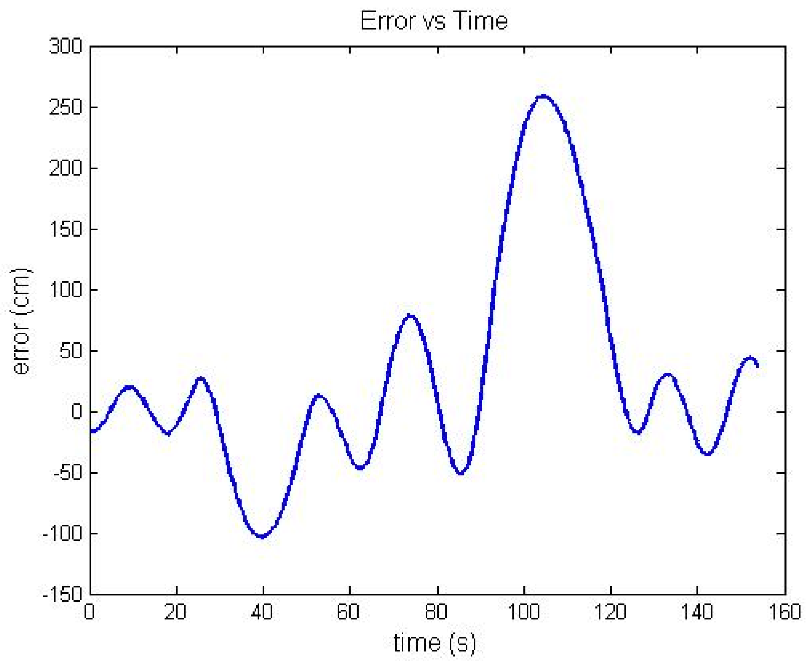

Figure 4.18: Path Following Error (third run at 0.5 m/s)

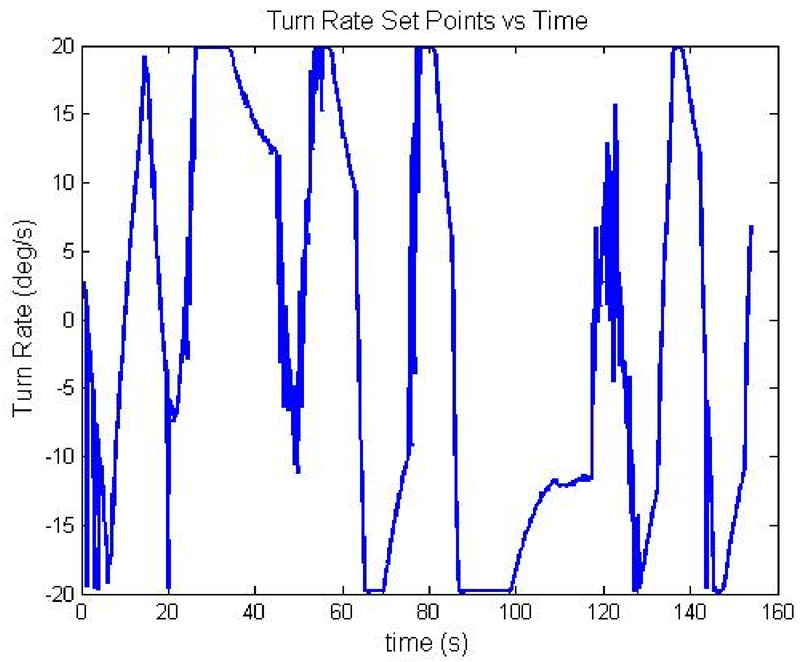

Figure 4.19: Set Points (third run at 0.5 m/s)

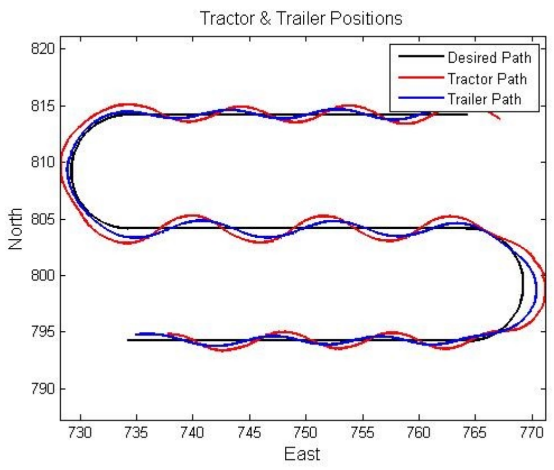

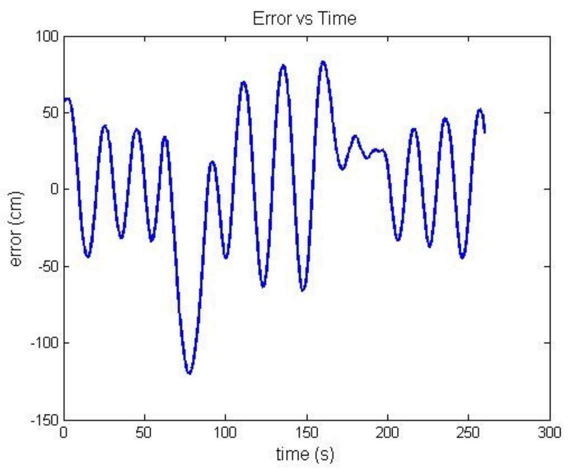

Figure 4.20: Results with 4m prediction horizon, weighted

4.3.1 Controller Tuning

To help examine the performance of the controller, the straight sections of the S-curve were widened from 12 meters to 30 meters. For safety reasons, the speed of the tractor was limited to 0.5 meters. Initially, a prediction horizon of 4 meters was chosen, and each prediction point was weighted by scaling them heavier near the trailer, and scaling them lighter away from the trailer, as shown in Table 4.3:

Distance from Robot	Scale Factor
1 meter	$\sqrt{4}$
2 meters	$\sqrt{3}$
3 meters	$\sqrt{2}$
4 meters	$\sqrt{1}$

Table 4.3: Scale Factors

With a 4 meter prediction horizon, weighted using the scale factors of Table 4.3, a path following performance shown in Figure 4.20 results. While these controller parameters worked fine in simulation, they produce unstable results on the physical robot.

Next, a 4 meter horizon without weights was tried, as shown in Figure 4.21. The results suggest that the controller is no longer unstable, but there is no evidence that the controller would reach steady state.

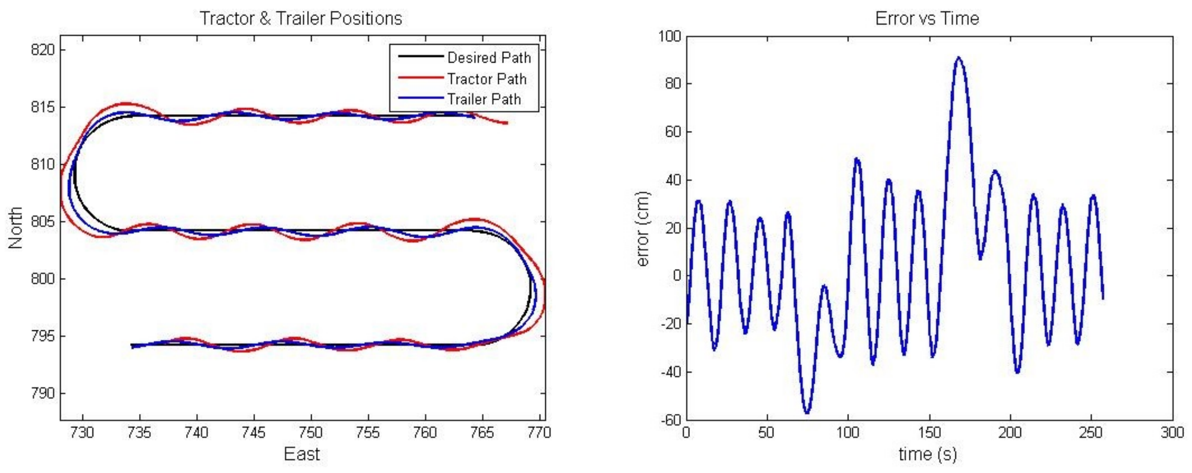

Figure 4.21: Results with 4m prediction horizon, unweighted

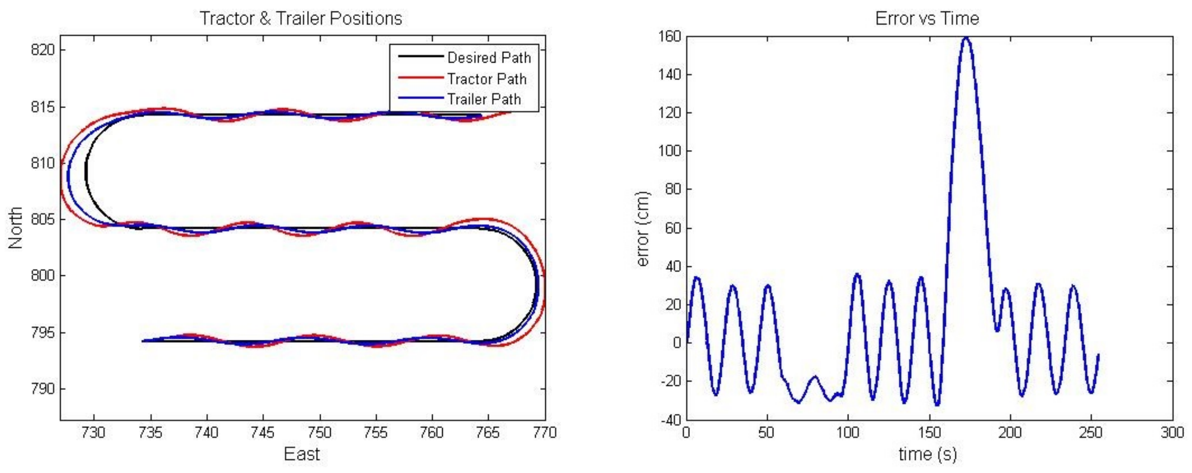

Figure 4.22: Results with 5m prediction horizon, weighted

The prediction horizon was then adjusted from 4 meters to 5 meters. Figure 4.22 shows the performance under a weighting scheme similar to Table 4.3. Similarly to the unweighted 4m horizon trial in Figure 4.21, there is no evidence that the controller would reach steady state.

Next, the weights were removed from the 5 meter prediction horizon. Figure 4.23 shows the robot tracking much better to the path under these conditions. These results suggest that the robot would eventually reach steady state.

So far, the results shown have suggested that by lengthening the prediction horizon and weighing it so that its "center" is further away from the trailer, the controller tracks better.

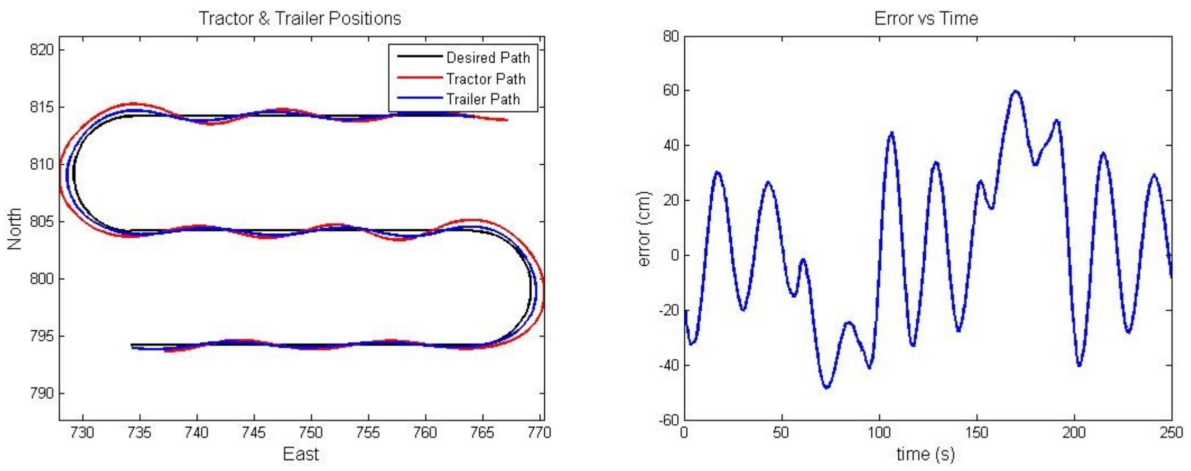

Figure 4.23: Results with 5m prediction horizon, unweighted

With that in mind, a prediction horizon of 6 meters was tried, but it failed as the computer speed of the robot was not fast enough to process the calculations in time. To compensate for this limitation, the 5 meter horizon was kept, but the weighting of the prediction points was shifted forward by using the scaling factors in Table 4.4:

Distance from Robot	Scale Factor
1 meter	$\sqrt{1}$
2 meters	$\sqrt{2}$
3 meters	$\sqrt{3}$
4 meters	$\sqrt{4}$
5 meters	$\sqrt{5}$

Table 4.4: Inverted Scale Factors

Figure 4.24 shows the robot performance with a prediction horizon of 5 meters, using this inverted weighing scheme. Now, the robot converges onto the path much more quickly, and the oscillations appear to have a half-life of roughly 25 meters.

Next, the horizon was reduced back to 4 meters, and the same inverted weighting scheme was used. The results, shown in Figure 4.25, show that the oscillations converge more slowly than with the 5 meter horizon. It should be noted that when using the 4 meter horizon with the inverted weighting, as well as when using the unweighted 5 meter horizon, the trailer tracked the turns better than with the 5 meter horizon with inverted weighting.

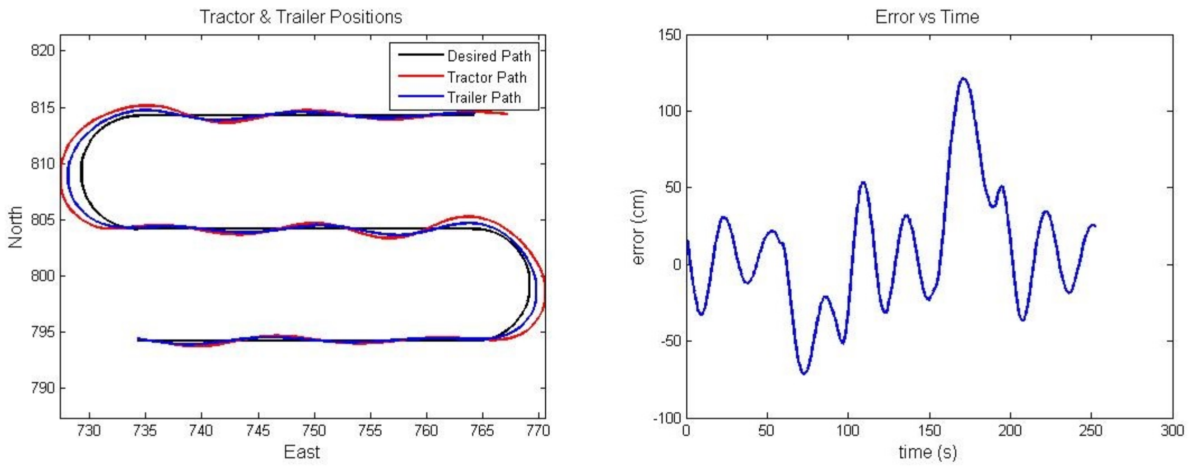

Figure 4.24: Results with 5m prediction horizon, weighted inversely

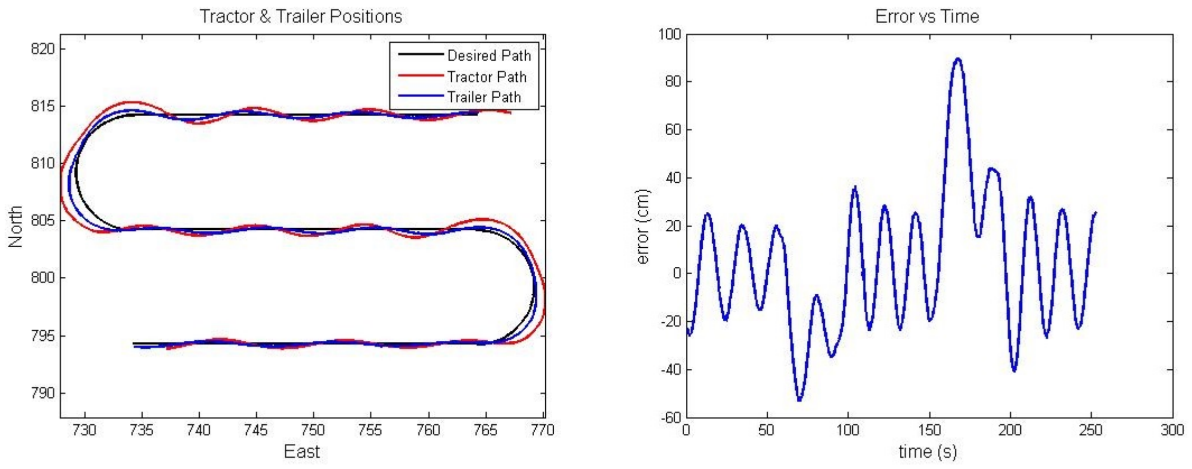

Figure 4.25: Results with 4m prediction horizon, weighted inversely

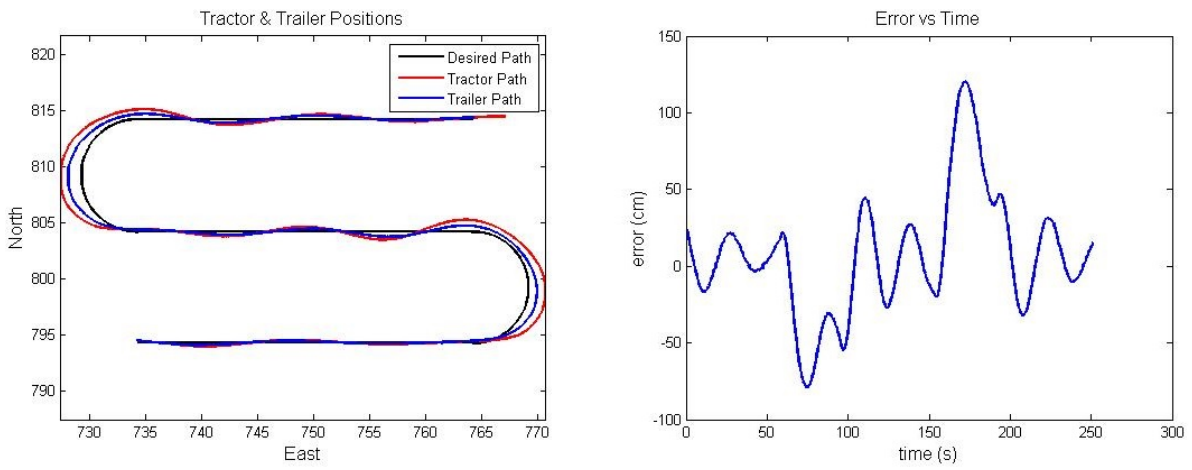

Figure 4.26: Results with 5m prediction horizon, weighted inversely, one-to-one

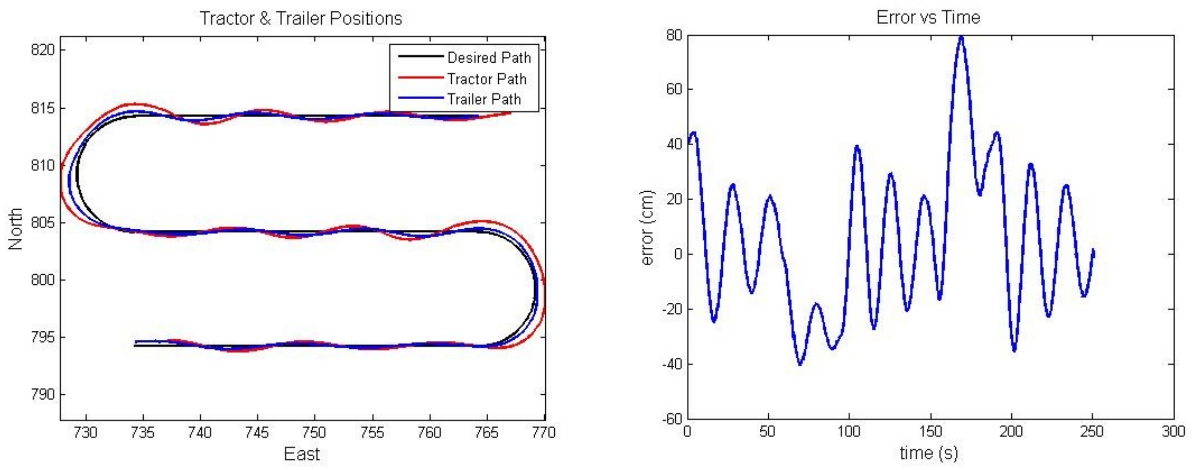

Figure 4.27: Results with 4m prediction horizon, weighted inversely, one-to-one

Finally, a one-to-one horizon weighting scheme was chosen, illustrated in Table 4.5:

Distance from Robot	Scale Factor
1 meter	1
2 meters	2
3 meters	3
4 meters	4
5 meters	5

Table 4.5: Inverted Scale Factors, One-to-One

Figures 4.26 and 4.27 show the results under the one-to-one weighting scheme. From these results, it is found that the 4 meter prediction horizon produces the most accurate

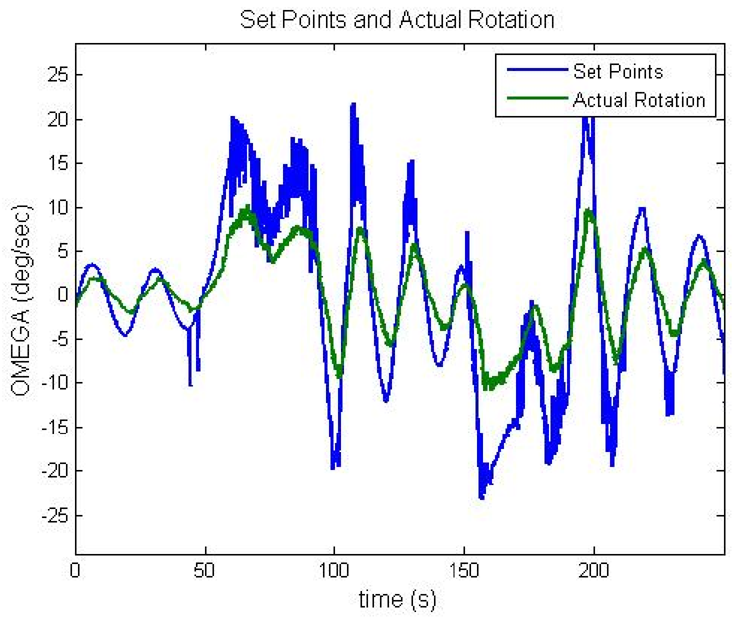

Figure 4.28: Turn Rates at 0.5 m/s

path following on the turns, while the 5 meter prediction horizon shows a faster progression toward steady state and more gradual oscillations. It is also seen that regardless of the weighting configuration, the error is still much higher than previous controllers. Subsection 4.3.2 examines the reason for this.

4.3.2 Turn Rate Analysis

After examining the desired turn rates chosen by the controller against the actual turn rates produced by the robot, it was found that the robot was only turning at roughly 40% to half the intended turn rate. Figures 4.28 and 4.29 show this discrepancy for the robot traveling at 0.5 m/s and 1.0 m/s, respectively.

In addition to this scaling discrepancy, the input-output plot shows roughly a 1.5-2 second delay in the response. To better understand the robot response, another test was done where the robot was given a step input turn rate command of 0.5 rad/sec. As seen in Figure 4.30, the delay could be modeled as a first order lag with a time constant of 0.5 seconds.

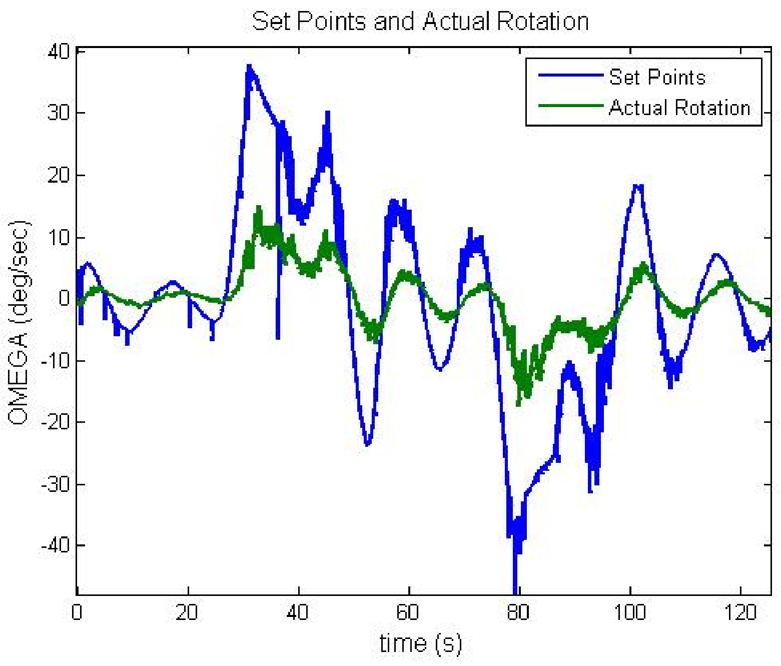

Figure 4.29: Turn Rates at 1.0 m/s

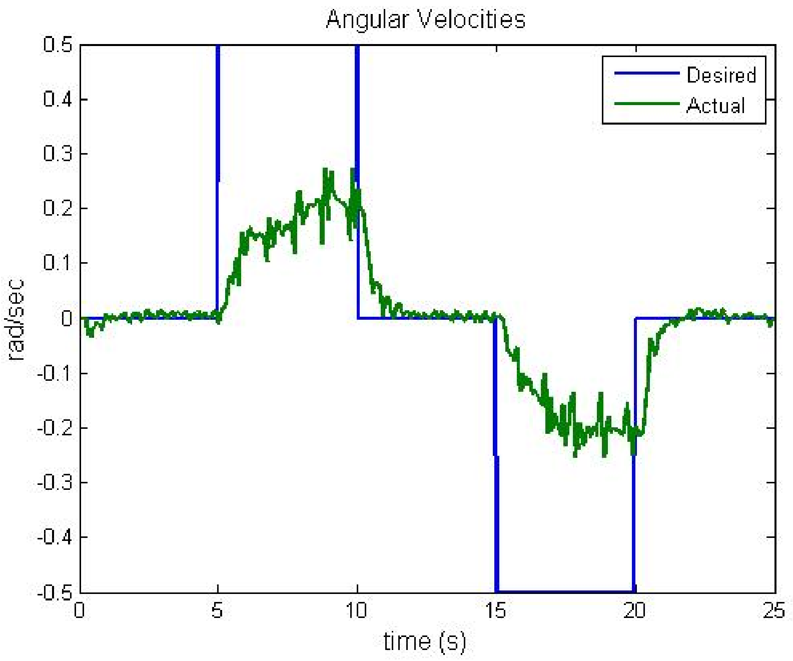

Figure 4.30: Turn Rate Step Input Response

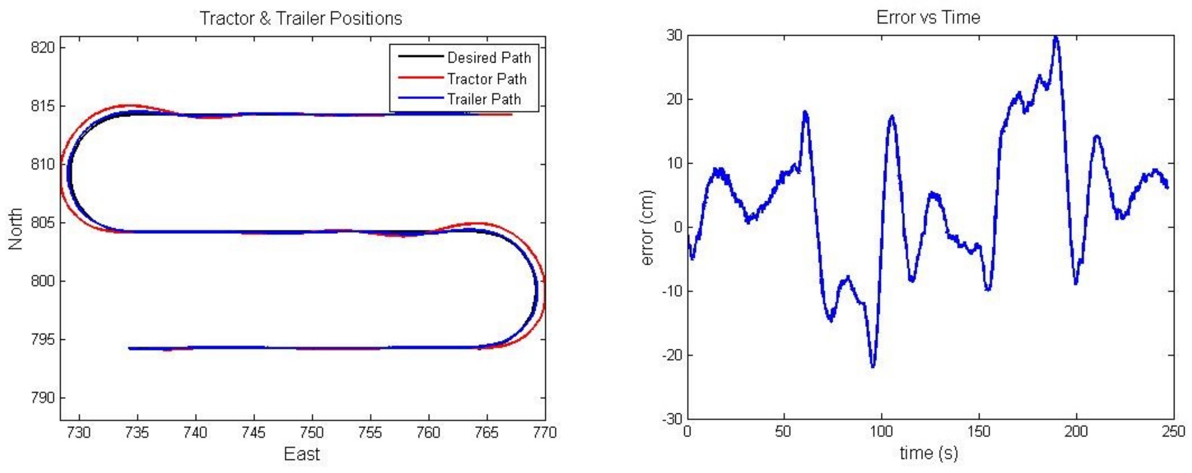

Figure 4.31: Path Following at 0.5 m/s

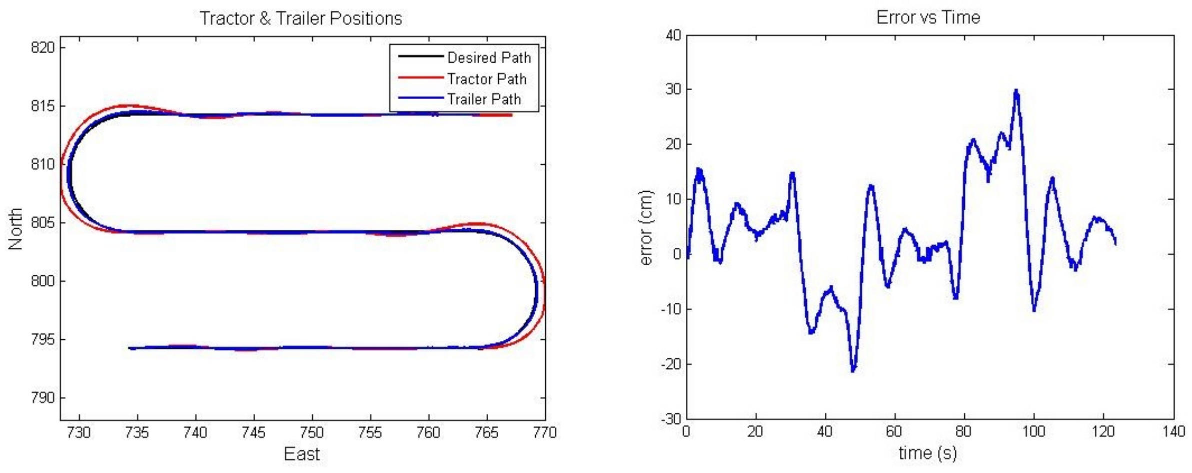

Figure 4.32: Path Following at 1.0 m/s

4.3.3 Applying the Scale Factor to the Input

Using the one-to-one weighting scheme, and scaling the intended values of the robot input by a factor of 2, the robot's path following improved dramatically. Figures 4.31 and 4.32 show the robot following the path at 0.5 m/s and 1.0 m/s respectively, with a maximum error of 30 cm on the turns and 15 cm on the recovery. They also shows that the robot recovers to steady state after about 1.5 oscillations. However, for unknown reasons, there consistently appears to be a bias of 5 cm in the error measurements as the robot travels East.

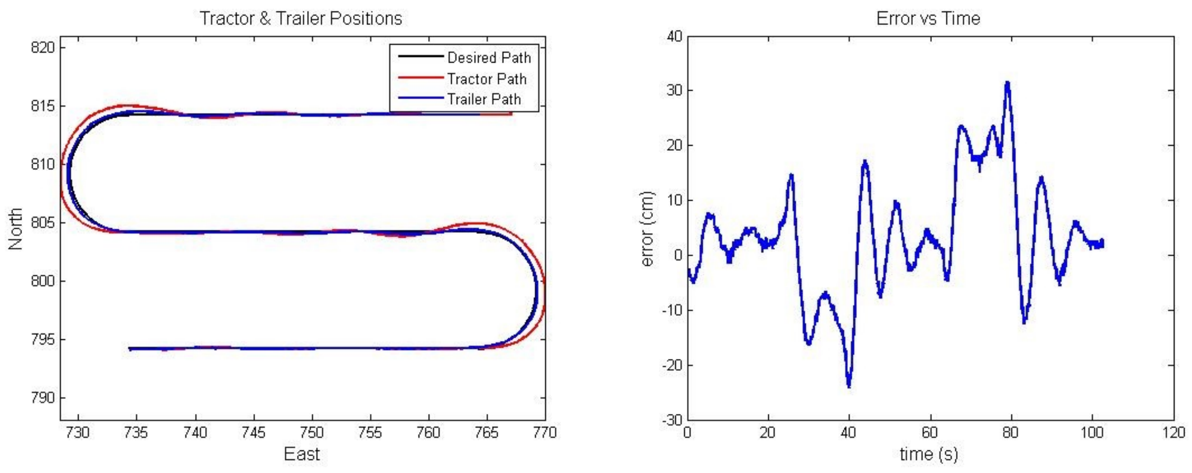

Figure 4.33: Path Following at 1.2 m/s

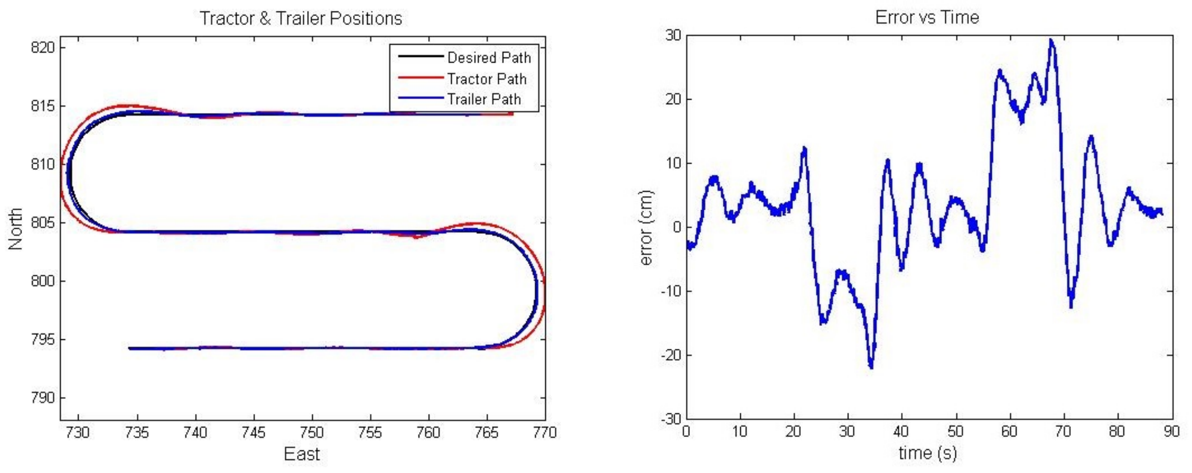

Figure 4.34: Path Following at 1.4 m/s

Next, the run was repeated using forward velocities between 1 and 2 m/s, increasing the forward velocity in 0.2 m/s intervals. Figures 4.33 through 4.37 show how the controller begins to lose its ability to reach steady state at 1.6 m/s.

So far, all tests have used a prediction model that assumes an immediate robot response to a command. Further improvements might be made by factoring a first order lag with a 0.5 second time constant into the steer input of prediction model, or by designing a phase lead compensator for the input [19].

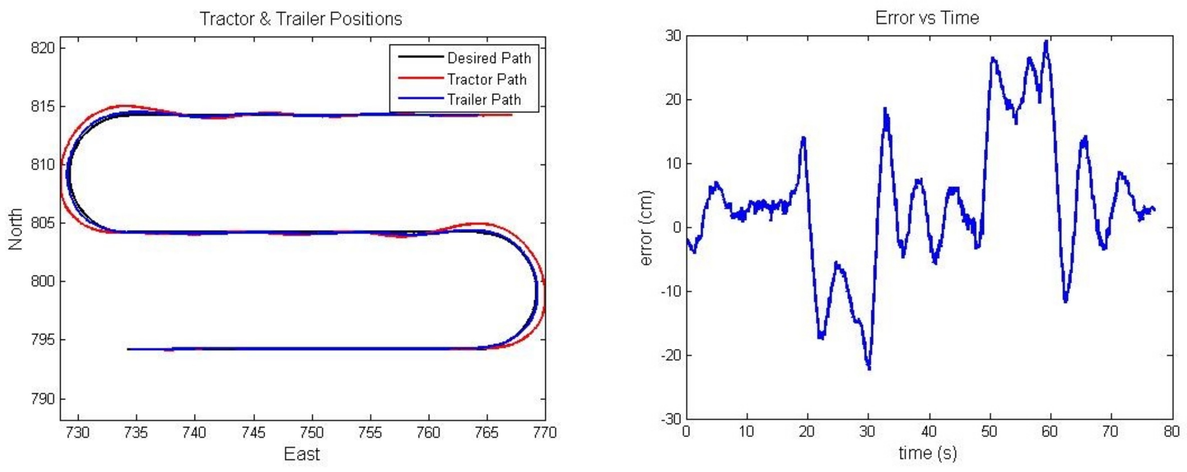

Figure 4.35: Path Following at 1.6 m/s

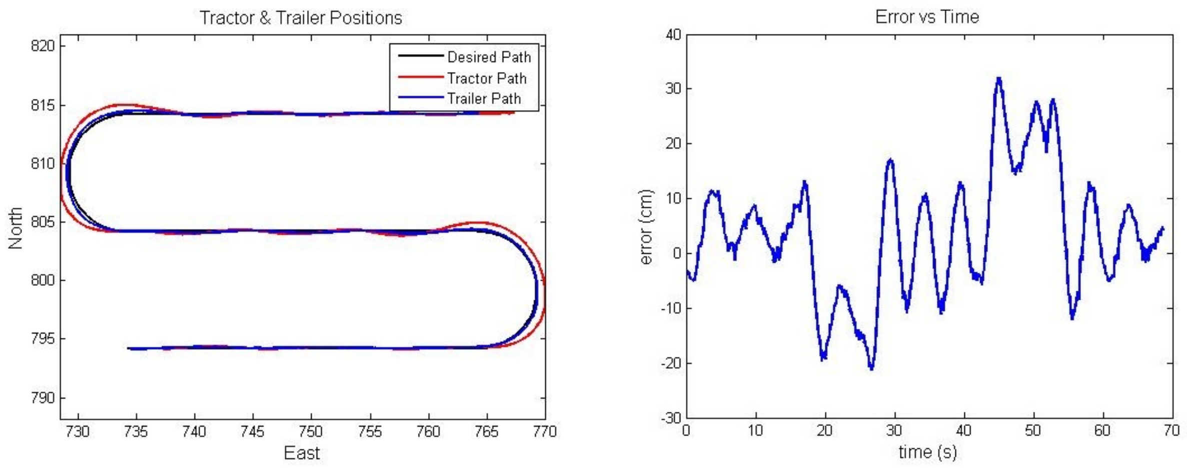

Figure 4.36: Path Following at 1.8 m/s

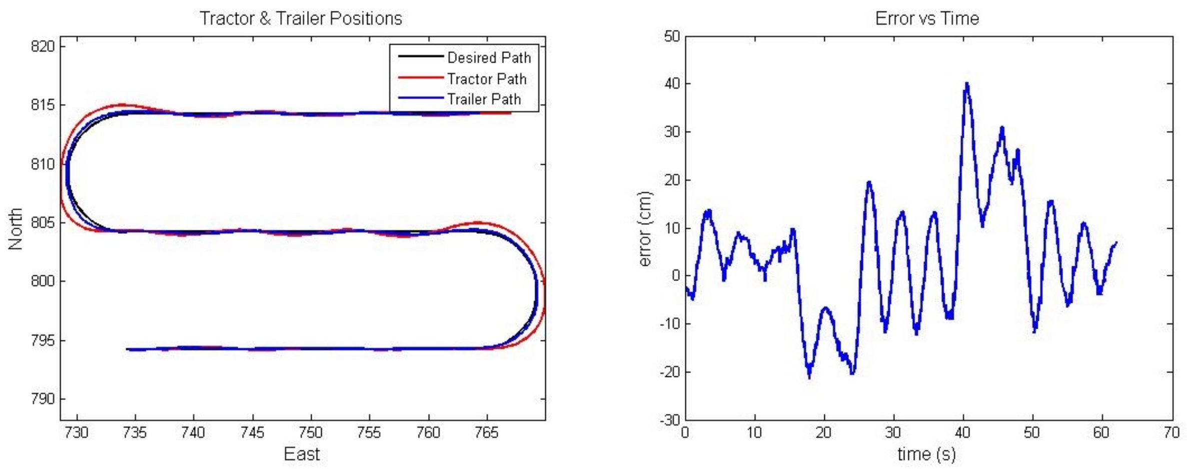

Figure 4.37: Path Following at 2.0 m/s

4.4 Conclusion

This chapter presented the results from simulation tests in Matlab and the ROS-based simulator, as well as results from the live run. So far, the results have shown that the performance of this controller is comparable to the linear controller used at Auburn University. If the system lag of the robot were factored into the model, the controller would likely perform even better.

In addition, the results show that the horizon length and prediction weighting have a significant effect on controller performance. Shorter horizons with heavier weighting on the earlier predictions produce better path following on turns, but the controller tends to overcorrect on the straight sections. Longer horizons with heavier weighting on the later predictions allow for a better recovery on the straight sections, but the path following becomes less accurate on the turns. In future work, perhaps the controller code could be rewritten so that the horizon length and weighting would self-adjust based on the curvature of the path in front of the trailer, as was studied in [20].

Chapter 5
Summary and Conclusion

Improvements in the field of tractor-trailer control are ongoing at Auburn University. In this thesis, the author presented a derivation of two models – a kinematic model and a bicycle model. While the bicycle model allows for adjustments regarding turn responsiveness and tire stiffness, the high demand on computing speed makes its feasibility questionable using present computer technology. This could, however, change in a few years as computer processor speeds increase.

Next, a model predictive control strategy was presented that numerically computes a target steer angle (or turn rate for a skid-steer robot) that would keep the trailer as close to the path as possible over a given prediction horizon. To achieve the steer angle, classical control methods, such as a PID controller, can be applied.

The thesis concludes with simulation and experimental results, both in the lab and in the field. First, the results of using the kinematic model for the controller against the bicycle model were presented to simulate how the controller would react to model error. Next, results from a live run on the Segway were presented. The simulation results showed that the error can be as little as 8.5 cm with a highly accurate model. The live data showed that this controller can still function with model inaccuracies, and the maximum error was typically around 29 cm on the turns, and 15 cm on the recovery. Incorporating system lag into the prediction model should further improve the performance of the controller, but it will have to be considered future work.

Other future work in this field would include model validation of the bicycle tractor-trailer model, trying the bicycle model as a control model, as well as trying different tire models, as faster computing technology becomes available. Another way to improve the

Segway path following performance would be to try different skid-steer vehicle dynamic models that account for tire slip. The overall goal is to someday use a model that produces a highly accurate and robust control system performance without overwhelming the time limits of the processor speed. Finding a balance between an accurate model and a reliable control method that is fast enough to implement in real-time would enable vehicle dynamics and control engineers to design autonomous vehicle systems to track a path to new levels of accuracy.

Appendix A

Model Predictive Control - A General Case

Model Predictive Control resembles Linear Quadratic Regulation (LQR), in that a cost function is first defined and minimized in order to find the desired input to a system. The general form for this cost function is defined by Equation (A.1).

$$J = \sum_{j=1}^{N} \left[Q_j \left(r_j - x_j \right)^2 + R_j \Delta u_j^2 \right] \tag{A.1}$$

There are several methods to finding the minimum of this cost function. What follows in this chapter is an algorithm for linear systems [15]. For non-linear systems, such as the tractor-trailer setup, several methods have been tried, including the method described in this thesis.

A Linear MPC Algorithm

A linear system in state space takes the following form:

$$x_{k+1} = A_d x_k + B_d u_k + w_k \tag{A.2}$$

$$y_{k+1} = C_d x_{k+1} \tag{A.3}$$

To implement MPC, first the system matrices are augmented to create integration variables.

$$A_d \to \begin{bmatrix} A_d & 0 \\ C_d & I \end{bmatrix} B_d \to \begin{bmatrix} B_d \\ 0 \end{bmatrix} C_d \to \begin{bmatrix} C_d & 0 \end{bmatrix} x_k \to \begin{bmatrix} x_k \\ x_I \end{bmatrix} \tag{A.4}$$

Also define:

$$e_k = \begin{bmatrix} w_k \\ -y_{ref} \end{bmatrix} Q_x = \begin{bmatrix} C^T Q_y C & 0 \\ C & Q_I \end{bmatrix} R_x = R_y \tag{A.5}$$

The predictor can be set up in a matrix format by taking a recursive approach:

$$x_{k+1|k} = A_d x_k + B_d u_k + w_k$$

$$x_{k+2|k} = A_d^2 x_k + A_d B_d u_k + B_d u_{k+1|k} + w_k + w_{k+1|k}$$

$$...$$

$$x_{k+\lambda|k} = A_d^{\lambda} x_k + A_d^{\lambda-1} B_d u_k + ... + B_d u_{k+\lambda-1} + w_k + ... + w_{k+\lambda-1|k}$$

Now, a new family of matrices can be defined:

$$Z = \begin{bmatrix} A_d \\ A_d^2 \\ ... \\ A_d^{\lambda} \end{bmatrix} M = \begin{bmatrix} I & 0 & 0 & 0 \\ A_d & I & 0 & 0 \\ ... & ... & I & 0 \\ A_d^{\lambda-1} & ... & A_d & I \end{bmatrix} V = \operatorname{diag}\begin{pmatrix} B_d & ... & B_d \end{pmatrix} \tag{A.6}$$

$$X = \begin{bmatrix} x_{k+1|k} \\ \vdots \\ x_{k+\lambda|k} \end{bmatrix} X^{ref} = \begin{bmatrix} x^{ref}_{k+1|k} \\ \vdots \\ x^{ref}_{k+\lambda|k} \end{bmatrix} U = \begin{bmatrix} u_k \\ \vdots \\ u_{k+\lambda-1|k} \end{bmatrix} E = \begin{bmatrix} e_k \\ \vdots \\ e_{k+\lambda-1|k} \end{bmatrix} \tag{A.7}$$

$$Q = \operatorname{diag}\begin{pmatrix} Q_x & ... & Q_x \end{pmatrix} R = \operatorname{diag}\begin{pmatrix} R_x & ... & R_x \end{pmatrix} \tag{A.8}$$

The gain is computed as follows:

$$L = \left(R + (MV)^T QMV\right)^{-1} (MV)^T Q \tag{A.9}$$

The control input is then found:

$$U = -LZx_k + Lx^{ref} - LME \tag{A.10}$$

After the control input applied to the system variable k is advanced by 1, the new states are observed, and the prediction matrix is updated:

$$X = Zx_k + MVU + ME \tag{A.11}$$

Now, Equations (A.9), (A.10), and (A.11) may be repeated indefinitely, or until the desired state is achieved.

Appendix B

Bicycle Model State Equations, Separated by State Variable

In Chapter 2, five state equations were derived for a tractor-trailer bicycle model with tire slip. These equations were presented as follows:

$$m_1\ddot{y}_1 + m_2\ddot{y}_2\cos\Delta - m_2\ddot{x}_2\sin\Delta = F_{y1} - m_1\dot{x}_1 r_1 + F_{y2} - \left(m_2\dot{x}_2 r_2 - F_{y3}\right)\cos\Delta - m_2\dot{y}_2 r_2\sin\Delta \tag{B.1}$$

$$I_1\dot{r}_1 - cm_2\ddot{y}_2\cos\Delta + cm_2\ddot{x}_2\sin\Delta = aF_{y1} - bF_{y2} + c\left(m_2\dot{x}_2 r_2 - F_{y3}\right)\cos\Delta + cm_2\dot{y}_2 r_2\sin\Delta \tag{B.2}$$

$$dm_2\ddot{y}_2 - I_2\dot{r}_2 = (d+e)\,F_{y3} - dm_2\dot{x}_2 r_2 \tag{B.3}$$

$$\ddot{y}_1\sin\Delta - c\dot{r}_1\sin\Delta + \ddot{x}_2 = -\dot{x}_1 r_1\sin\Delta - \left(\dot{y}_1 r_1 - cr_1^2\right)\cos\Delta + \dot{y}_2 r_2 + dr_2^2 \tag{B.4}$$

$$\ddot{y}_1\cos\Delta - c\dot{r}_1\cos\Delta - \ddot{y}_2 - d\dot{r}_2 = -\dot{x}_1 r_1\cos\Delta + \left(\dot{y}_1 r_1 - cr_1^2\right)\sin\Delta + \dot{x}_2 r_2 \tag{B.5}$$

In addition, the tire slip forces were defined as follows:

$$F_{y1} = C_1\arctan\left(\frac{-\dot{x}_1\sin\left(\beta_1+\delta\right) + \dot{y}_1\cos\left(\beta_1+\delta\right) + ar_1\cos\delta}{\dot{x}_1\cos\left(\beta_1+\delta\right) + \dot{y}_1\sin\left(\beta_1+\delta\right) + ar_1\sin\delta}\right)\cos\delta \tag{B.6}$$

$$F_{y2} = C_2 \arctan\left(\frac{-\dot{x}_1 \sin\beta_1 + \dot{y}_1 \cos\beta_1 - br_1}{\dot{x}_1 \cos\beta_1 + \dot{y}_1 \sin\beta_1}\right) \tag{B.7}$$

$$F_{y3} = C_3 \arctan\left(\frac{-\dot{x}_2 \sin\beta_2 + \dot{y}_2 \cos\beta_1 - er_2}{\dot{x}_2 \cos\beta_2 + \dot{y}_2 \sin\beta_2}\right) \tag{B.8}$$

It was noted that the five states could be isolated using Cramer's Method. To help limit the algebra, the right-hand side of each equation will be redefined as follows:

$$A = F_{y1} - m_1\dot{x}_1 r_1 + F_{y2} - (m_2\dot{x}_2 r_2 - F_{y3})\cos\Delta - m_2\dot{y}_2 r_2 \sin\Delta \tag{B.9}$$

$$B = aF_{y1} - bF_{y2} + c\,(m_2\dot{x}_2 r_2 - F_{y3})\cos\Delta + cm_2\dot{y}_2 r_2 \sin\Delta \tag{B.10}$$

$$C = (d+e)\,F_{y3} - dm_2\dot{x}_2 r_2 \tag{B.11}$$

$$D = -\dot{x}_1 r_1 \sin\Delta - \left(\dot{y}_1 r_1 - cr_1^2\right)\cos\Delta + \dot{y}_2 r_2 + dr_2^2 \tag{B.12}$$

$$E = -\dot{x}_1 r_1 \cos\Delta + \left(\dot{y}_1 r_1 - cr_1^2\right)\sin\Delta + \dot{x}_2 r_2 \tag{B.13}$$

Now, the system of equations is written as a matrix equation:

$$\begin{bmatrix} m_1 & 0 & m_2\cos\Delta & 0 & -m_2\sin\Delta \\ 0 & I_1 & -cm_2\cos\Delta & 0 & cm_2\sin\Delta \\ 0 & 0 & -dm_2 & I_2 & 0 \\ \sin\Delta & -c\sin\Delta & 0 & 0 & 1 \\ \cos\Delta & -c\cos\Delta & -1 & -d & 0 \end{bmatrix} \begin{bmatrix} \ddot{y}_1 \\ \dot{r}_1 \\ \ddot{y}_2 \\ \dot{r}_2 \\ \ddot{x}_2 \end{bmatrix} = \begin{bmatrix} A \\ B \\ C \\ D \\ E \end{bmatrix} \tag{B.14}$$

Taking the determinant of the left-hand 5x5 matrix will give the denominator of each state variable solution:

$$den = -I_1 I_2 (m_1 + m_2) - I_2 m_2 d^2 \left(m_1 + m_2 \sin^2 \Delta\right) - m_1 m_2 c^2 \left(m_2 d^2 \sin^2 \Delta + I_2\right) \tag{B.15}$$

To get the numerator for each state variable, the right-hand column vector is substituted into the state variable's corresponding column the left-hand 5x5 matrix, and the determinant is taken. In other words, substituting into the first column and taking the determinant would produce the numerator for the first state variable, while substituting into the second column would produce the numerator for the second state variable, and so on.

For $\ddot{y}_1$, the solution would look as such:

$$\ddot{y}_1 = \frac{\begin{vmatrix} A & 0 & m_2 \cos\Delta & 0 & -m_2 \sin\Delta \\ B & I_1 & -c m_2 \cos\Delta & 0 & c m_2 \sin\Delta \\ C & 0 & -d m_2 & I_2 & 0 \\ D & -c \sin\Delta & 0 & 0 & 1 \\ E & -c \cos\Delta & -1 & -d & 0 \end{vmatrix}}{den} \tag{B.16}$$

For $\dot{r}_1$, the solution would be:

$$\dot{r}_1 = \frac{\begin{vmatrix} m_1 & A & m_2 \cos\Delta & 0 & -m_2 \sin\Delta \\ 0 & B & -c m_2 \cos\Delta & 0 & c m_2 \sin\Delta \\ 0 & C & -d m_2 & I_2 & 0 \\ \sin\Delta & D & 0 & 0 & 1 \\ \cos\Delta & E & -1 & -d & 0 \end{vmatrix}}{den} \tag{B.17}$$

and so on.

The solutions come out to be the following:

$$\ddot{y}_1 = \frac{-A\left[m_2\left(I_1c^2 + m_2c^2d^2\sin^2\Delta + I_1d^2\right) + I_1I_2\right] - Bm_2c\left(I_2 + m_2d^2\sin^2\Delta\right) - I_1m_2\left[(Cd + EI_2)\cos\Delta + D\left(m_2d^2 + I_2\right)\sin\Delta\right]}{-I_1I_2\left(m_1 + m_2\right) - I_2m_2d^2\left(m_1 + m_2\sin^2\Delta\right) - m_1m_2c^2\left(m_2d^2\sin^2\Delta + I_2\right)} \tag{B.18}$$

$$\dot{r}_1 = \frac{-Am_2c\left(I_2 + m_2d^2\sin^2\Delta\right) - B\left[m_2\left(I_2 + m_2d^2\sin^2\Delta + m_1d^2\right) + m_1I_2\right] + c\left[(C + EI_2m_1m_2)\cos\Delta + Dm_1m_2\left(I_2 + m_2d^2\right)\sin\Delta\right]}{-I_1I_2\left(m_1 + m_2\right) - I_2m_2d^2\left(m_1 + m_2\sin^2\Delta\right) - m_1m_2c^2\left(m_2d^2\sin^2\Delta + I_2\right)} \tag{B.19}$$

$$\ddot{y}_2 = \frac{Cd\left[m_1\left(I_1 + m_2c^2\sin^2\Delta\right) + m_2I_1\sin^2\Delta\right] + I_2\left\{\left[Bm_1c - Dm_2\left(m_1c^2 + I_1\right)\sin\Delta\right]\cos\Delta + \left[Em_1\left(I_1 + c^2m_2\sin^2\Delta\right) - I_1\left(A\cos\Delta - Em_2\sin^2\Delta\right)\right]\right\}}{-I_1I_2\left(m_1 + m_2\right) - I_2m_2d^2\left(m_1 + m_2\sin^2\Delta\right) - m_1m_2c^2\left(m_2d^2\sin^2\Delta + I_2\right)} \tag{B.20}$$

$$\dot{r}_2 = \frac{(Bm_1m_2cd - AI_1m_2d)\cos\Delta - C\left[m_2\left(m_1c^2 + I_1\right) + I_1m_1\right] - \frac{1}{2}Dm_2^2d\left(I_1 + m_1c^2\right)\sin 2\Delta + Edm_2\left[I_1m_1 + \left(I_1 + m_1c^2\right)m_2\sin^2\Delta\right]}{-I_1I_2\left(m_1 + m_2\right) - I_2m_2d^2\left(m_1 + m_2\sin^2\Delta\right) - m_1m_2c^2\left(m_2d^2\sin^2\Delta + I_2\right)} \tag{B.21}$$

$$\ddot{x}_2 = \frac{\left(I_2 + m_2d^2\right)(AI_1 - Bm_1c)\sin\Delta + \frac{1}{2}\left(Cm_2d + EI_2m_2\right)\left(I_1 + m_1c^2\right)\sin 2\Delta - D\left[I_1I_2\left(m_1 + m_2\cos^2\Delta\right) + m_1m_2\left(I_1d^2 + I_2c^2\cos^2\Delta\right)\right]}{-I_1I_2\left(m_1 + m_2\right) - I_2m_2d^2\left(m_1 + m_2\sin^2\Delta\right) - m_1m_2c^2\left(m_2d^2\sin^2\Delta + I_2\right)} \tag{B.22}$$

Bibliography

[1] P. Falcone, F Borrelli, H. E. Tseng, J. Asgari, D. Hrovat. *A Hierarchical Model Predictive Control Framework for Autonomous Ground Vehicles.* American Controls Conference, 2008.

[2] H. H. Nelson, J. R. McDonald. *Multisensor towed array detection system for UXO detection.* Geoscience and Remote Sensing, IEEE Transactions on 39.6 (2001): 1139-1145, 2001.

[3] B. Lepore, Defense Capabilities and Management. *GAO-12-709R Military Base Realignments and Closures.* Memorandum to the United States Government and Accountability Office, 2012.

[4] L. Dubins. *On curves of minimal length with a constraint on average curvature, and with prescribed initial and terminal positions and tangents.* American Journal of Mathematics 79, pp. 497-516. The Johns Hopkins University Press, 1957.

[5] D. M. Bevly, B. Parkinson *Carrier-Phase Differential GPS for Control of a Tractor Towed Implement.* Proceedings of the 13th International Technical Meeting of the Satellite Division of The Institute of Navigation (ION GPS 2000) pp. 2263-2268, Salt Lake City, UT, September 2000.

[6] T. C. Ng, J. Guzman, M. Adams. *Autonomous vehicle-following systems: A virtual trailer link model.* Intelligent Robots and Systems, 2005 IEEE/RSJ International Conference, pp. 3057-3062, IEEE, 2005.

[7] L. Z. Wang, et al. *An approximation approach of the clothoid curve defined in the interval [0, $\pi/2$] and its offset by free-form curves.* Computer-Aided Design 33.14 (2001): 1049-1058, 2001.

[8] Seborg, Edgar, Mellichamp. *Process Dynamics and Control*, 2nd ed. Wiley 2003

[9] D. Hodo. *Development of an Autonomous Mobile Robot-Trailer System for UXO Detection.* MS Thesis, Auburn University, 2007.

[10] M. Payne. *Non-Collocated Control of an Autonomous Vehicle-Trailer System Using State Estimation.* MS Thesis, Auburn University, 2012.

[11] A. Singh. *Nonlinear Control of a Robot-Trailer System Using a Hybrid Backstepping-linearizing approach.* MS Thesis, Auburn University, 2012.

[12] D. Karnopp. *Vehicle Stability.* Marcel Dekker, 2004.

[13] D. Karnopp, D. Margolis. *Engineering Applications of Dynamics.* Wiley, 2008.

[14] L. Alexander, M. Donath, M. Hennessey, V. Morellas, C. Shankwitz. *A Lateral Dynamic Model of a Tractor-Trailer: Experimental Validation.* University of Minnesota & the Minnesota Department of Transportation, 1996.

[15] P. Malaterre, and J. Rodellar. *Design and comparison of multivariable optimal and predictive controllers on a 2-pool irrigation canal.* Journées Hispano-Françaises Systèmes In- telligents & Contrôle Avancé, Laboratoire Européen Asso- cié, UPC Barcelona, 1996.

[16] S. Chapra, R. Canale. *Numerical Methods for Engineers, 6th ed.* McGraw Hill, 2010.

[17] R. Larson, B. Edwards, D. Falvo. *Elementary Linear Algebra, 5th ed.* Houghton Mifflin Company, 2004.

[18] D. Hodo, et. al. *Morse Blender Simulator for Differential Steering Robot.* Morse, 2011.

[19] W. Woodall. *Low-Bandwidth Three Dimensional Mapping and Latency Reduction Model Prediction to Improve Teleoperation of Robotic Vehicles.* MS Thesis, Auburn University, 2012.

[20] J. Backman, T. Oksanen, A. Visala. *Nonlinear Model Predictive Trajectory Control in Tractor-Trailer System for Parallel Guidance in Agricultural Field Operations.* Agricontrol, 2010.